

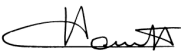




Preliminary Thermal and Structural Design of the PHENIX FVTX Detector System

LANS Sub-Contract #38694-001-06 33

Eric Ponslet, Shahriar Setoodeh, Roger Smith
4/24/2007

| | Name | Phone & E-Mail | Signature |
|---------------|-----------------------------------|---|--|
| Main Authors: | Eric Ponslet Shahriar Setoodeh | (505) 661-3000 ponslet@hytecinc.com, ext. 15 setoodeh@hytecinc.com, ext. 31 |   |
| Approved: | Eric Ponslet | ponslet@hytecinc.com, 505-661-3000, ext 15 |  |

Abstract

This document summarizes the preliminary design of the structural support and cooling of the PHENIX Forward Vertex Detector (FVTX). Design requirements are summarized, the design is described in detail, and numerical and analytical predictions of performance are presented.

This document and the associated preliminary drawings constitute the final deliverables for contract number 38694-001-06 33 between Los Alamos National Security (LANS), LLC and HYTEC, Inc., entitled "Mechanical Engineering Support for the Pioneering High Energy Nuclear Interaction Experiment (PHENIX) Forward Vertex Detector (FVTX)".

DESIGN ENGINEERING
ADVANCED COMPOSITE APPLICATIONS
ULTRA-STABLE PLATFORMS

110 EASTGATE DR.
LOS ALAMOS, NM 87544

PHONE 505 661-3000
FAX 505 662-5179



Revision Log

| Rev. | Date | Author(s) | Summary of Revisions/Comments |
|------|----------|---|-------------------------------|
| - | 04/24/07 | E. Ponslet, S. Setoodeh, R. Smith | Original Release |

Table of Contents

| | |
|---|-----------|
| Abstract..... | 1 |
| Revision Log..... | 2 |
| Table of Contents | 3 |
| 1. Introduction..... | 5 |
| 1.1 Background | 5 |
| 1.2 Overview of Conceptual Design | 5 |
| 2. Design Requirements & Specifications..... | 8 |
| 2.1 Coordinate System..... | 8 |
| 2.2 FVTX geometry | 9 |
| 2.3 Envelope | 9 |
| 2.4 Sensor Module Specifications..... | 10 |
| 2.5 Design Life..... | 11 |
| 2.6 Environment..... | 11 |
| 2.6.1 Dry gas enclosure | 11 |
| 2.6.2 Temperature and humidity in experiment hall (outside gas enclosure) | 11 |
| 2.6.3 Radiation | 11 |
| 2.6.4 Magnetic field | 11 |
| 2.6.5 Vibration and acoustic disturbances..... | 12 |
| 2.6.6 Other environmental loads | 12 |
| 2.7 Modularity..... | 12 |
| 2.8 Grounding | 12 |
| 2.9 Initial Alignment and Surveying, and Dimensional Stability..... | 12 |
| 2.10 Power Dissipation and Temperature Limits..... | 12 |
| 2.11 Stiffness and Natural Frequency..... | 13 |
| 2.12 Radiation length..... | 13 |
| 3. Trade and Design Studies..... | 14 |
| 3.1 Introduction | 14 |
| 3.1.1 Key issues..... | 14 |
| 3.1.2 Modeling approach | 14 |
| 3.2 Wedge trade studies | 14 |
| 3.2.1 Backplane material..... | 14 |
| 3.2.2 Backplane thickness and layup..... | 21 |
| 3.2.3 Module to station thermal interface..... | 21 |
| 3.3 Half-disk assembly | 22 |
| 3.4 Half-Arm Assembly..... | 23 |
| 4. Preliminary Design Description | 25 |
| 4.1 Modular Design Approach | 25 |
| 4.1.1 Sensor modules | 25 |
| 4.1.2 Half-stations | 26 |
| 4.1.3 Half-arm assembly | 26 |
| 4.2 Sensor Module..... | 26 |
| 4.2.1 Backplane..... | 27 |
| 4.2.2 Bond design..... | 28 |
| 4.2.3 Assembly approach | 29 |
| 4.3 Half-Station Sub-Assembly | 30 |
| 4.3.1 Support panel construction..... | 31 |
| 4.4 Half-Arm Sub-Assembly..... | 33 |
| 4.5 Cooling System..... | 34 |

| | |
|---|-----------|
| 4.5.1 Gas enclosure | 34 |
| 4.5.2 Active cooling of FVTX stations | 34 |
| 4.5.3 Cooling tube..... | 36 |
| 4.5.4 Module to panel thermal bridge | 37 |
| 4.5.5 Cooling circuit..... | 38 |
| 5. Preliminary Design: Performance Predictions..... | 39 |
| 5.1 Cooling System..... | 39 |
| 5.1.1 Flow rate of coolant | 39 |
| 5.1.2 Cooling tube to bulk fluid temperature drop | 40 |
| 5.1.3 Temperature drops from tube wall to backplane | 40 |
| 5.1.4 Pressure drop..... | 41 |
| 5.1.5 Effect of natural convection into dry gas..... | 42 |
| 5.2 Radiation Length Percentage | 43 |
| 5.3 Radiation Hardness | 46 |
| 5.4 Detector Module Performance | 46 |
| 5.5 Half-Station Performance..... | 47 |
| 5.6 FVTX Half-Station | 49 |
| 5.7 VTX/FVTX System Level Analysis..... | 50 |
| 6. Conclusions..... | 52 |
| 6.1 Remaining issues..... | 53 |
| 6.1.1 Known issues and/or concerns with the preliminary design..... | 53 |
| 6.1.2 Remaining tasks for final design phase | 54 |
| 6.2 Recommended Future Work (Short Term) | 55 |
| 6.2.1 Prototyping..... | 55 |
| 6.2.2 Design: | 56 |
| 6.2.3 Other: | 56 |
| 7. Related HYTEC Documents..... | 57 |
| 7.1 Presentation Slides..... | 57 |
| 7.2 Preliminary Drawing Package | 57 |
| 8. References | 58 |
| 9. Acronyms..... | 59 |
| <i>Appendix A. Material properties used in models.....</i> | <i>61</i> |
| <i>Appendix B. Mass properties.....</i> | <i>63</i> |
| <i>Appendix C. 2-D vs. 3-D Wedge Results</i> | <i>64</i> |
| <i>Appendix D. Analytical Validations.....</i> | <i>66</i> |
| <i>Appendix E. Statement of Work.....</i> | <i>68</i> |

1. Introduction

1.1 Background

This document summarizes the work performed by HYTEC, Inc, under subcontract number 38694-001-06 33 between Los Alamos National Security (LANS), LLC and HYTEC, Inc., entitled “Mechanical Engineering Support for the Pioneering High Energy Nuclear Interaction Experiment (PHENIX) Forward Vertex Detector (FVTX)”. Together with the Preliminary Drawing Package (Section 7.2), it constitutes the final deliverable for completion of this contract.

The statement of work for this contract (Appendix E) included the following general tasks:

- Structural and thermal design of FVTX sensor internal support and cooling hardware, including sensor module, station, and half-arm designs
- Design of cooling system, integrated with the above, to control the temperature of the sensors and FPHX chips
- Project management, travel, and procurement of materials as needed

These tasks have been completed as summarized in this report.

1.2 Overview of Conceptual Design

The Forward VerTeX (FVTX) detector is one of two inner silicon detector systems planned for the PHENIX upgrade to be installed at Brookhaven National Laboratory’s RHIC (Relativistic Heavy Ion Collider) facility around 2009-2010. The general configuration of PHENIX is illustrated in Figure 1.

Together, the VerTeX (VTX) and FVTX detectors combine into the so-called Multiplicity/Vertex Detector (MVD, Figure 2) and provide the innermost detection and tracking of particles produced by the interaction. The VTX consists of a system of four concentric “barrels” of silicon pixel and strip detectors that track particles emanating for the interaction at the steeper angles. The FVTX detector “caps” those barrels to track particles emanating at shallower angles.

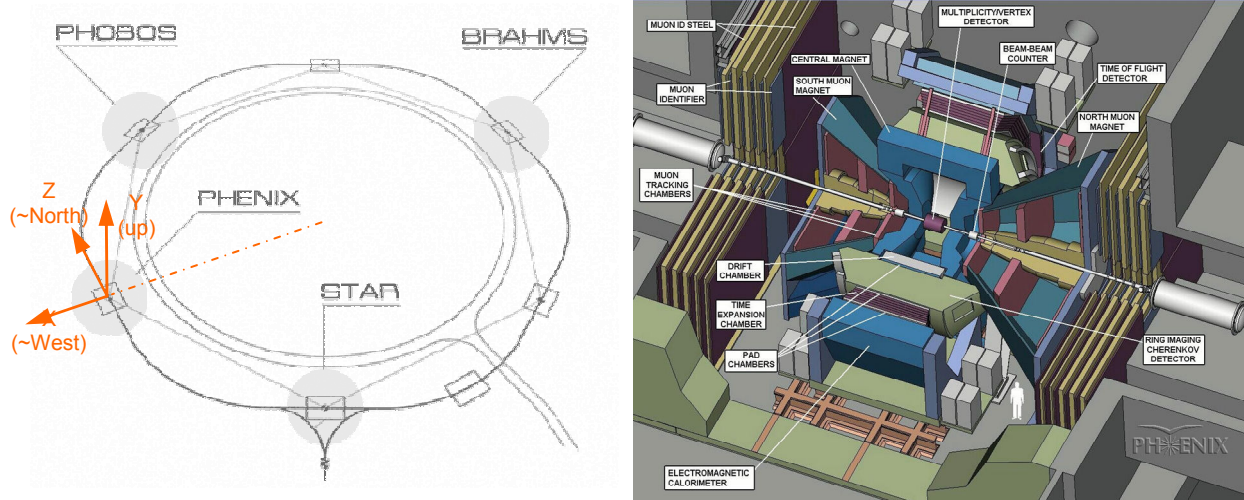


Figure 1: Location of the PHENIX detector along the RHIC (left) and configuration of detector systems within PHENIX (right).

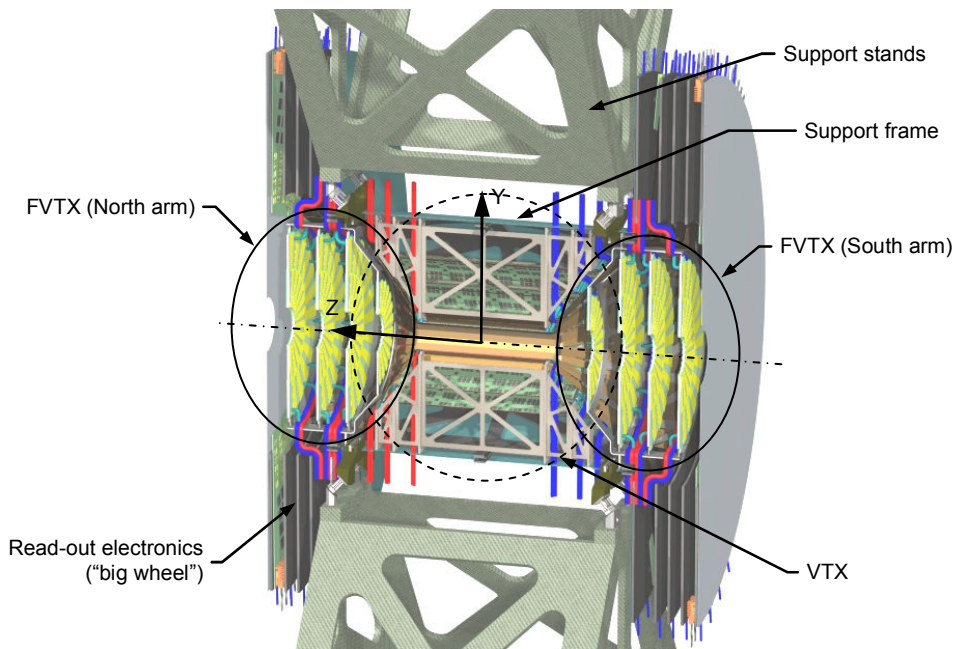


Figure 2: General configuration of the inner detectors (MVD) for the upcoming PHENIX upgrade.

The FVTX consists of two identical arms (North/+Z and South/-Z). Each arm consists of four, generally planar detector stations, orthogonal to the beam trajectory, and spaced about 55mm from one another. The stations are numbered 1 to 4 within each arm, starting from the station closest to the interaction point (IP).

Each FVTX station provides near hermetic coverage of silicon strip detectors, over the entire 360° azimuthal range. Hermetic coverage is achieved by populating both sides (upstream and

downstream) of each station with partial-coverage silicon sensors, and staggering those detectors in azimuth between the two sides to achieve full coverage.

Because the detector systems (both VTX and FVTX) must be assembled around a pre-installed beryllium beam pipe, they are being designed in two halves, split about a vertical plane going through the centerline of the beam pipe. This “clam shell” design results in each FVTX arm being constructed from two halves, each consisting of 4 half-stations supported by a half-shell support structure.

Before assembly around the beam pipe, a half-VTX and two FVTX half-arms are integrated together into two identical assemblies. Both detector subsystems are mechanically supported by a barrel-shaped support frame made from lightweight graphite composite sandwich panels. This frame is itself supported by two metal stands (located at the top and bottom of the detector system), which mount on four I-beams, connected to the magnet poles. Kinematic mounts are used to decouple the graphite frame from the metallic supports.

Stations 2, 3, and 4 of the FVTX are identical to one another. Their active sensor areas extend from an inner radius of approximately 45mm to an outer radius of about 172mm. Packaging and geometric concerns dictate that station 1 (closest to the interaction point) must be smaller; its outer radius is about 105mm.

The basic building block of the FVTX is the sensor module (a.k.a. “wedge”). Each module is designed to fully support a single sensor. It includes the sensor itself, the front-end chips (shaping amplifiers and ADCs, integrated into an ASIC, which is referred to as the FPHX chip), a flexible printed circuit board, and connectors. The module is built onto a *backplane*, which provides both mechanical support and passive conductive cooling.

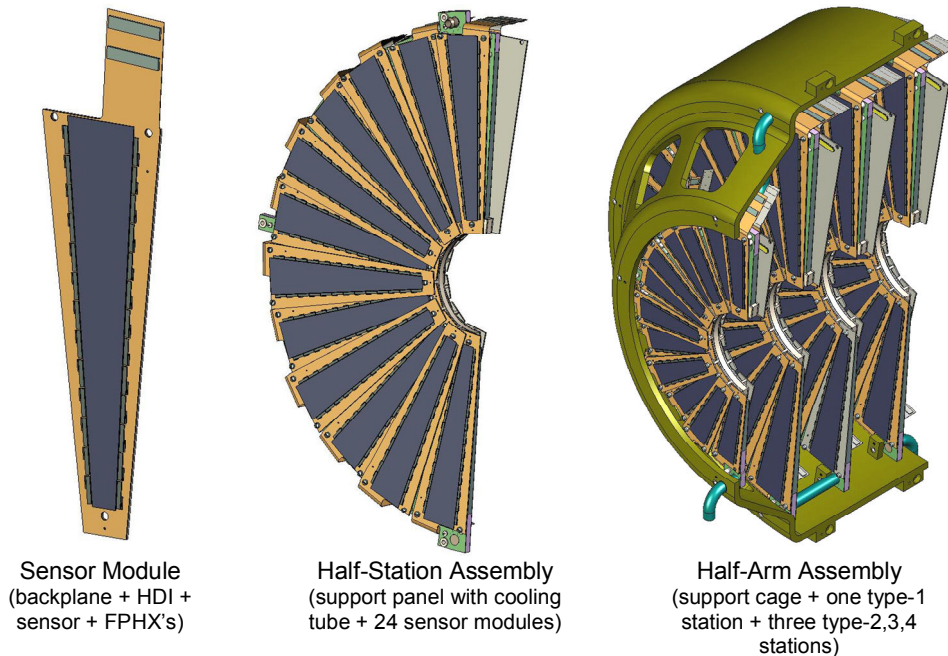


Figure 3: Basic components and sub-assemblies of the FVTX

The entire FVTX is built from only two different wedge designs: one for station 1, and the other for the larger stations 2, 3, and 4. A half-station is assembled by fastening 12 sensor modules on each side of a structural support panel, shaped as a half-circular disk. The support panel is made from a lightweight composite sandwich. A cooling tube is integrated into the support panel, near the outer edge. A single-phase, liquid coolant is pumped through this tube at a controlled temperature, to remove waste heat from the FPHX chips, and maintain them and the sensor modules at a constant temperature. Thermal contact between the outer edge of the wedge backplanes and the support panel and its cooling tube is achieved with a compliant conductive adhesive.

2. Design Requirements & Specifications

A draft requirements document^[1] was prepared by M. Brooks, the FVTX project manager, on January 26, 2007. That first draft did not include radiation length or temperature requirements. These aspects of the designs were developed based on informal, mostly oral exchanges between HYTEC and project personnel, primarily at LANL.

A revised requirement document^[2] was obtained from M. Brooks on April 5, 2007, after the preliminary design had been frozen, and while this report was being prepared. Therefore, the designs presented herein were developed based on the draft requirements, specifically:

- in the absence of a limit on radiation length, and,
- without a specified upper limit on the temperature of the sensors or FPHX chips (the design is based on an upper limit of about room temperature ($\sim 21^{\circ}\text{C}$) that was arrived at in discussions with various members of the FVTX collaboration; that limit was eventually confirmed in Version 2 of the Design Document^[2]).

Most of the requirements listed below are taken from the draft requirements document^[1]. Some additional requirements have been compiled from various written and oral communications between HYTEC and the FVTX collaboration. Some have evolved over time. The numbers listed in this section are HYTEC's best understanding of the requirements as of the date of publication of this document. When they differ from the numbers used during the design phase, numbers from the final design requirement document are also listed (for reference only since the design was based on the January 26, 2007 draft).

2.1 Coordinate System

The FVTX will be designed and analyzed in the PHENIX coordinate system, which is defined as follows^[2 and 3], and illustrated in Figure 1:

- the origin is at the nominal interaction point (which is also at the geometric center of the inner vertex detector system and in the plane of symmetry between the two arms of the FVTX).
- the X axis is perpendicular to the RHIC orbit at the interaction point, in a radial direction from the RHIC ring center. The positive direction is radially outward (West).
- the Y axis points vertically upward.

- the Z axis is aligned with the RHIC orbit and points North, in accordance with the right hand rule.

2.2 FVTX geometry

Figure 4 shows the axial (Z) locations of the four FVTX stations.

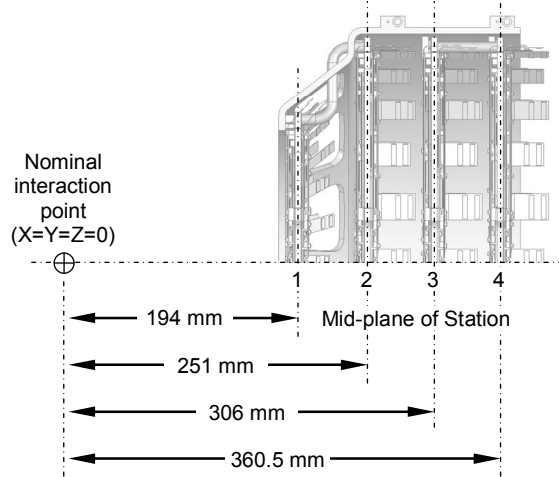


Figure 4: Baseline locations of FVTX stations^[11] (rounded to the nearest ½ mm)

The radial extent of the active areas of the FVTX stations^[12] results from the dimensions of the sensors (Section 2.4) and from positioning the inner edge of the active area tangent to a cylinder of 45mm radius, whose axis is coincident with the Z axis.

2.3 Envelope

The VTX and FVTX are required to fit entirely within the envelope shown in Figure 5.

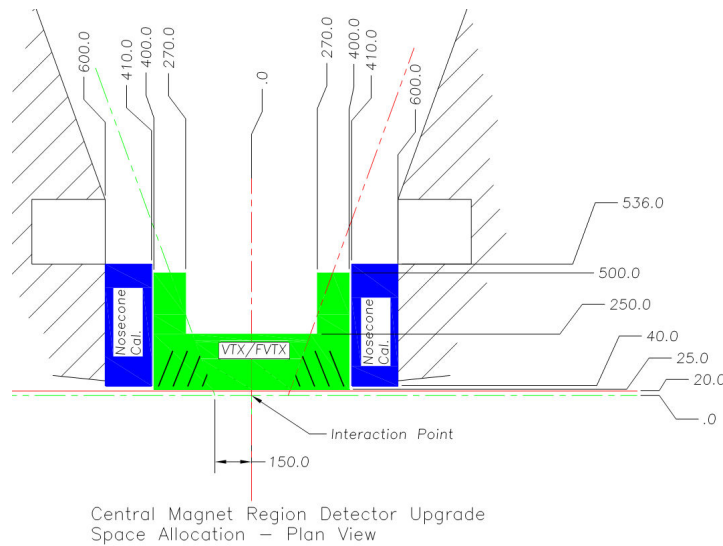


Figure 5: Space allocation for VTX and FVTX.

2.4 Sensor Module Specifications

The FVTX detector stations are equipped with silicon mini-strip sensors. Two different sizes of sensors are used: a large sensor is used in stations 2, 3, and 4, and a smaller version is used for station 1. The baseline dimensions of those two sensors and their active areas are shown in Figure 6.

The strips from each sensor in stations 2, 3, or 4 are read out by with 26 ADC chips (13 on each side of the wedge-shaped sensor) also referred to as FPHX chips. These chips are nominally 9mm long \times 1.5mm wide \times 300 μ m thick.

The same chips are used on the smaller station 1 modules, but their number is reduced to $12^{[8]}$ (6 on each side).

The sensor and the FPHX chips are mounted onto a High Density Interconnect (HDI), which is itself bonded to the wedge backplane. The HDI is a multi-layer (Kapton and copper) flexible printed circuit board; its detailed layer-by-layer specification^[6] is shown in Figure 7.

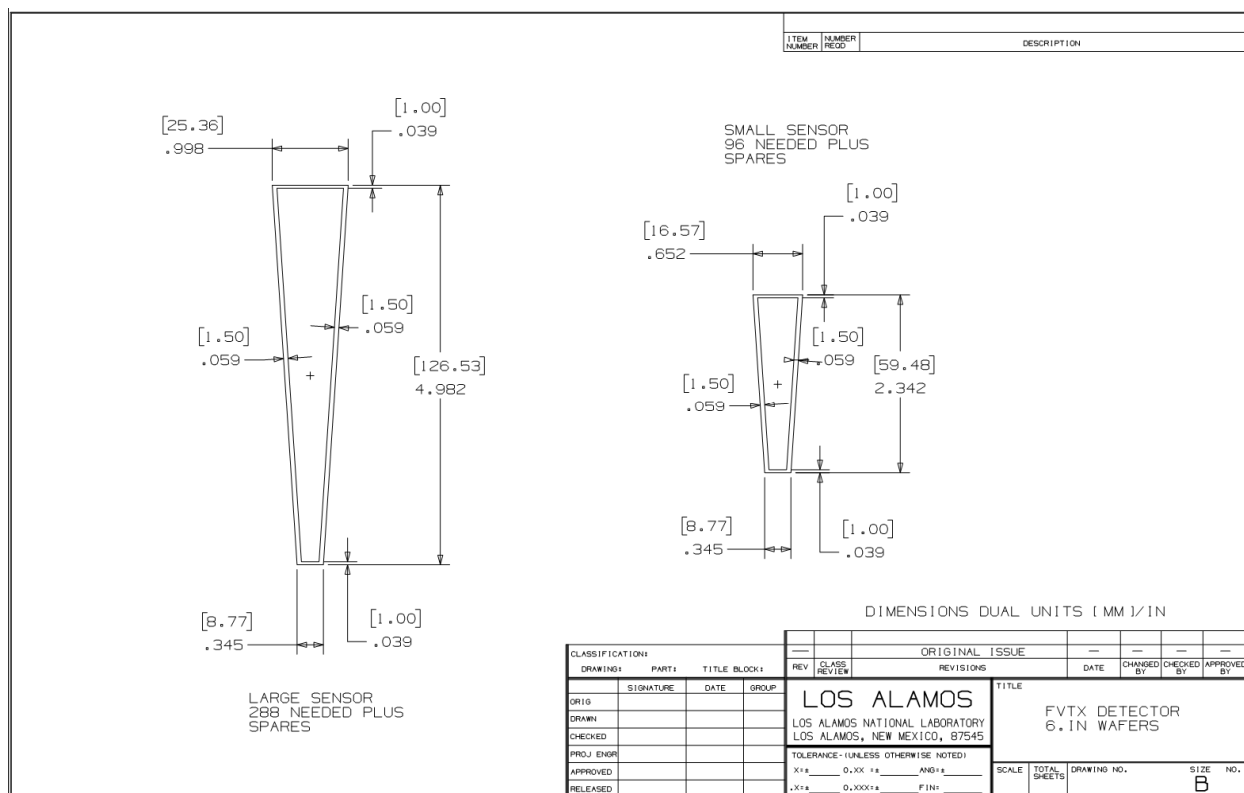


Figure 6: Baseline dimensions of FVTX sensors^[4].

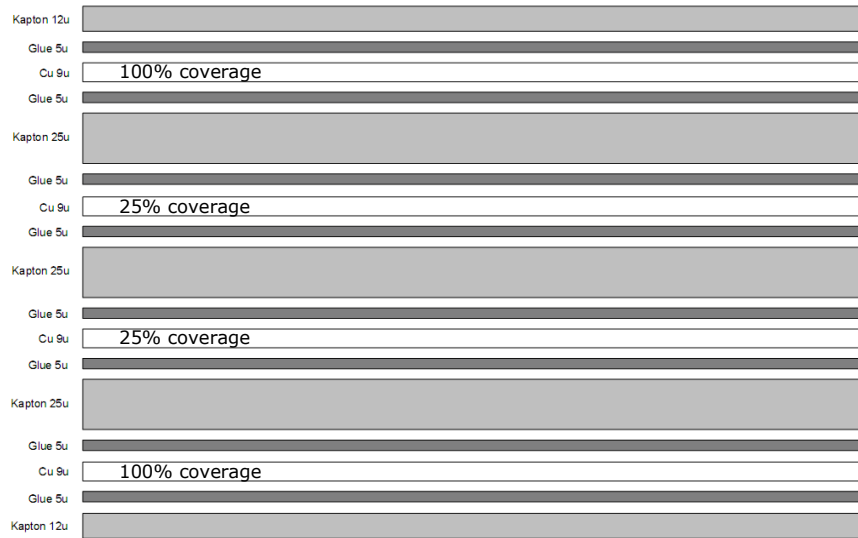


Figure 7: Layup specification of HDI^[6] (not to scale; thicknesses in microns; approximate coverage percentage of copper layers is also shown).

A minimum 4.0mm^[7] wide margin is required on the HDI, on either side of the sensor, for mounting the FPHX chips and decoupling capacitors, and for the wire-bonding pads from the FPHX chips to the HDI.

A minimum 2.5mm^[7] height clearance is required above the top surface of the HDI to any other hardware, for installation of the sensor, FPHX chips, decoupling capacitors, and wire bonds.

2.5 Design Life

All FVTX systems shall be designed for a useful life of 10 years.

2.6 Environment

2.6.1 Dry gas enclosure

The FVTX (at least the internal sensor systems) will be installed inside a gas enclosure. The enclosure will be purged with dry Nitrogen at a controlled temperature. That temperature is TBD but the current baseline is room temperature, 21°C. We suggest maintaining a tolerance of $\pm 2^\circ\text{C}$ on that temperature.

2.6.2 Temperature and humidity in experiment hall (outside gas enclosure)

The range of ambient temperature outside the enclosure is unspecified.

The range of humidity outside the enclosure is unspecified.

2.6.3 Radiation

The radiation dose will not exceed 200kRad^[1], integrated over the entire 10 year design life (i.e. 20kRad per year).

2.6.4 Magnetic field

The FVTX will experience a strong axial (parallel to Z) magnetic field. This field will not exceed 10,000 Gauss (1 Tesla)^[1].

2.6.5 Vibration and acoustic disturbances

Vibration background present on the magnet poles (to which the detector systems are attached), and acoustic inputs (into the gas enclosure) may be capable of exciting structural modes of the detector system, potentially leading to undesirable motion of the sensors. Although acoustic and vibration inputs are generally believed (by collaboration members) to be low enough not to be a concern, actual levels and frequency content are not specified.

2.6.6 Other environmental loads

Overload levels for design to seismic activity are not specified. The designs are therefore analyzed only for 1g static gravitational loading.

2.7 Modularity

The design should be as modular as practical to facilitate the integration and testing process and minimize wastage in case of component failures during integration and testing. In particular, individual sensor modules should – if at all possible – be individually replaceable^[5].

2.8 Grounding

Grounding requirements have not been specified.

2.9 Initial Alignment and Surveying, and Dimensional Stability

A complete description of these requirements is available in [1] (no changes in Version 2 of the same document^[2]). They are summarized in the table below.

| Type | Required Tolerance | |
|--|------------------------|--|
| | X, Y | Z |
| Initial Alignment (or surveying): | | |
| o Within station (alignment of detectors to station) | < $\pm 10\mu\text{m}$ | < $\pm 200\mu\text{m}$ ($\pm 75\mu\text{m}$ goal) |
| o Station position (including any rigid-body sag of the station) | < $\pm 200\mu\text{m}$ | < $\pm 200\mu\text{m}$ |
| Static Deformations (other than rigid body sag of a station) | < $\pm 10\mu\text{m}$ | < $\pm 14\mu\text{m}$ |
| Unsteady Deformations (vibrations) | < $\pm 10\mu\text{m}$ | < $\pm 14\mu\text{m}$ |

Table 1: Initial alignment or surveying accuracy, and dimensional stability requirements.

2.10 Power Dissipation and Temperature Limits

Each FPHX chip has 128 shaper amplifiers and ADC channels. Each channel dissipates $100\mu\text{W}$ of heat. This results in a total heat dissipation per sensor module of 0.333W for the larger modules of stations 2, 3, and 4, and 0.154W for the smaller station 1 modules. This power dissipation can be considered steady-state (i.e. negligible variations in power dissipation as a function of time, so that steady-state heat transfer is applicable after the initial power-up transient).

Power dissipation in the sensors is negligible.

The temperature of the sensors and FPHX chips must be maintained between some limits, both to avoid damage to the chips themselves, and to control background noise. Initially, the only requirements that were informally provided to us^[6] were to keep these temperatures between -10

and about +50°C. During a meeting on February 23, 2007, and in reaction to a predicted temperature of 27°C for the FPHX chips, the upper temperature limit was reduced to room temperature, to ease concerns about increased background noise. This new upper limit was later documented in Version 2 of the Design Document^[2].

2.11 Stiffness and Natural Frequency

No specific requirements are available. The fundamental frequency of the system should probably be kept high enough to keep the dynamic deflections of the response to any input (acoustic or from the base support, i.e. the magnet poles) small enough. Unfortunately, with no input specification available, we have no basis for deriving a natural frequency goal. If, on the other hand, vibrational and acoustic inputs are negligible, there is no other apparent reason to require a minimum value of the natural frequency of these detector systems.

Early in the project, a 70Hz minimum natural frequency had been suggested. This was motivated by a desire to stay well above any rotating machinery fundamental (about 30Hz), and the mains frequency of 60Hz. However, it quickly became evident that this frequency would not be attainable (at least at the system level), so the requirement was dropped and replaced with a goal of staying well above 30Hz. This requirement was never documented, and it is still arguable whether it is well founded. Better knowledge of the environmental disturbance sources (acoustic and base-vibration) would help us establish a firm value.

2.12 Radiation length

A radiation length requirement for the sensor support and cooling structures was not provided during the preliminary design phase. This resulted in some confusion about how much material would be acceptable, and how this varies for specific areas of the detector system.

An area-averaged* number became available in Version 2 of the Design Document^[2], unfortunately too late to guide the design (fortunately, it appears that – at least in terms of area-averaged RL – our design meets this requirement; see Section 5.2). The maximum allowable area-averaged* radiation length of an FVTX station (including sensors, FPHX chips, and HDI) is 2.74%^[2]. No guidance was provided about specific areas where more or less material may be allowable.

* The Design Document^[2] does not explicitly identify the limit as an area-averaged number. This interpretation is an assumption on our part.

3. Trade and Design Studies

3.1 Introduction

This section discusses some of the design history. It presents a number of studies that were performed to make educated decisions about key design features. Because these studies were obviously performed before the preliminary design was established, they do not all center around the same baseline. The particulars of the design baseline used for the various studies are listed in the corresponding sections. For final performance predictions of the preliminary design, please refer to Section 5.

Note also that our analyses focused exclusively on the larger modules of stations 2, 3, and 4. Since the power density on station 1 is very close to that of the other stations, and since both the heat transfer paths and structural spans are about half as long, the thermal and structural performance of station 1 and its components can be expected to exceed that of stations 2, 3, and 4.

3.1.1 Key issues

Some of the key questions in the early design studies had to do with the material selection and the required thickness for the module backplanes. Thermal pyrolytic graphite (TPG) had been suggested as a backplane material by others. We felt that the low heat flux and the high cost of TPG made that material both unnecessary and undesirable. Trade studies were conducted (and are summarized in this section) that justified selection of an appropriate alternative material.

3.1.2 Modeling approach

Numerical FE[†] models were first used to obtain steady-state temperature distributions of wedges based on the edge cooling design and heat generated in the FPHX chips. This temperature distribution was then used as a load to compute thermal distortions resulting from both the temperature gradient and the CTE mismatch between different materials in the wedge stack-up.

Since the FVTX disk assembly is installed in a vertical position, gravity sag is negligible compared to thermal distortions and will therefore be ignored throughout the following studies.

Finally, natural frequencies of wedges with different backplanes are obtained to examine whether resonance with an excitation at the site might be possible.

3.2 Wedge trade studies

3.2.1 Backplane material

The primary focus of the wedge trade studies is to investigate in-plane and through-the-thickness temperature gradients as a function of the backplane material. The 3-D model used in this section is not intended to accurately predict thermal distortions; results presented in this section are for relative comparisons only. More appropriate models will be used in the following sections for thermal distortion analyses.

[†] FEMAP 9.2 and NX Nastran 4 were used as analysis tools.

In the FE models, a wedge module has the following three different stack-ups:

- Active region: backplane/adhesive/HDI/adhesive/detector
- FPHX chip region: backplane/adhesive/HDI/thermally conductive adhesive/FPHX chips
- HDI region: backplane/adhesive/HDI

The backplane is used both as a structural element to support the electronics and sensors, and as a cold plate to spread the heat from the chips to the outer radius, where edge cooling is provided. The following different composite laminates are considered for the backplane

- TPG, encapsulated with $[0/90]_s$ M55J/954-3 facesheets
- $[0/45/90/-45]_s$ M55J/954-3 (Graphite/Cyanate composite)
- $[0/45/90/-45]_s$ K13C2U/RS-3C (Graphite/Cyanate composite)

Thermal pyrolytic graphite (TPG) is an advanced form of pyrolytic graphite with an extremely high in-plane thermal conductivity^[39] (about 1500 W/mK or almost 4 times that of pure copper). Depending on the input heat to the wedge and temperature requirements, TPG could be an excellent candidate for the backplane. Here we consider an encapsulated TPG core 0.246mm thick with $[0/90]_s$ facesheets resulting in a 0.5mm thick backplane. In addition to a TPG backplane, a typical mid-range quasi-isotropic Gr/CE laminate (M55J/954-3) and a high end fiber quasi-isotropic Gr/CE laminate (K13C2U/RS-3C) are also considered. K13C2U is an extremely high stiffness and thermal conductivity fiber. Fiber conductivity is about 620W/mK (almost twice that of pure copper). Typical real-world thermal conductivity of quasi-isotropic (QI) K13C2U resin bound laminates is around 180 W/mK (1/2 that of copper). Typical material properties for these backplanes are given in Appendix A.

The Kapton-Cu HDI laminate is glued to the backplane using a standard non-conductive, rigid epoxy adhesive. The silicon strip detector is in turn bonded to the HDI, also using a non-conductive epoxy. Finally, the FPHX chips are bonded to the HDI with a layer of thermally conductive epoxy to facilitate through the thickness heat transfer. Typical material properties along with their corresponding thicknesses used in numerical simulations are given in Table 14 in Appendix A.

Effective backplane properties for three different lay-ups described above are computed based on the classical lamination theory (CLT) and are given in Table 15 of Appendix A. These properties are used in 3-D solid modeling of the wedge. The CLT effective properties also provide a comparative measure for stiffness, CTEs, as well as thermal conductivities of different backplane material candidates.

A 3-D FE model was prepared to study thermal and structural responses of the wedge. Figure 8 depicts the 3-D mesh where each material layer is represented by two elements through the thickness. For example, the backplane is modeled using two solid elements through the thickness with effective *in-plane* properties. Effective in-plane properties will predict temperature distributions accurately; however, they are less accurate in thermal distortion calculations. This is explained by the fact that effective in-plane properties do not accurately represent flexural stiffness for composite materials. As a result, 3-D modeling is primarily used for steady-state heat transfer analysis. For more accurate thermal distortion predictions we rely on 2-D simulations with composite elements where each layer is modeled with orthotropic properties and its corresponding orientation angle. The 3-D model shown in Figure 8 has a total 156,708 nodes and 267,679 elements resulting in 470,124 degrees of freedom.

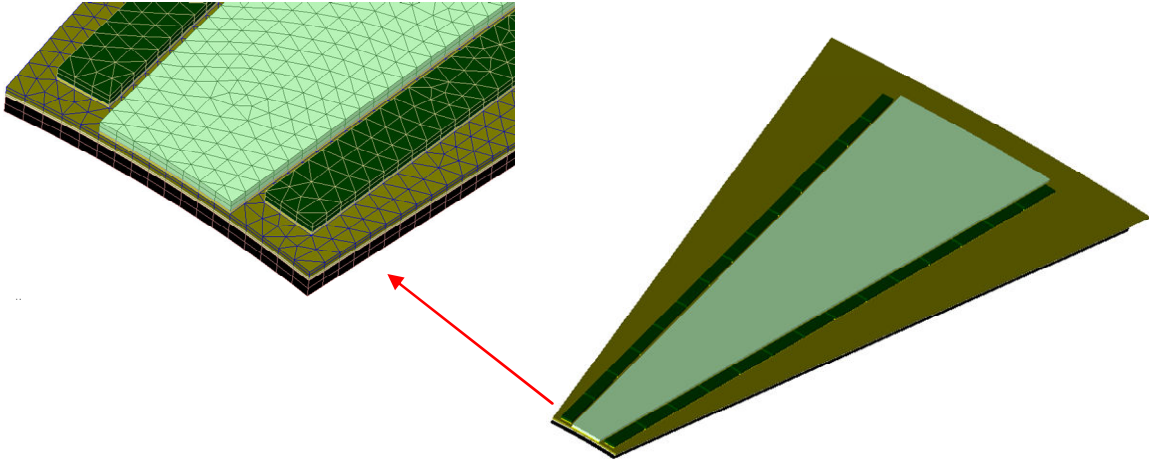


Figure 8: Schematic 3-D Finite Element Mesh.

For steady-state heat transfer analysis, it is assumed that waste heat is generated uniformly inside the FPHX chips. Table 2 summarizes calculation of the volumetric heat generation for each FPHX chip. The outer edge of the detector module is assumed to be cooled to 13°C along a 4.79mm wide strip of the back surface near the outer edge, where the cooling tube runs under the backplane (Figure 28).

| | | |
|----------------------------|-------------|------------------|
| Waste heat per channel | 100.00 | μW |
| Number of channels per ROC | 128 | |
| Waste heat per chip | 0.01280 | W |
| | | |
| Length | 0.00900 | m |
| Width | 0.00150 | m |
| Thickness | 0.00030 | m |
| Volume | 4.05000E-09 | m ³ |
| Heat Generation | 3.16049E+06 | W/m ³ |

Table 2: Volumetric FPHX chip heat generation

Structural supports are assumed to consist of three bolted connections^[18] to the support panel (Figure 20). One screw is at a radius of 41mm and the other two are located at a radius of 166.8mm. This connection is modeled using a spider of rigid elements spreading to a diameter of approximately 3.56mm, representative of the screw diameter. The center of this spider is fixed in three degrees of freedom. A schematic view of such a connection is shown in Figure 9 where the NASTRAN RBE2 rigid elements are shown in red.

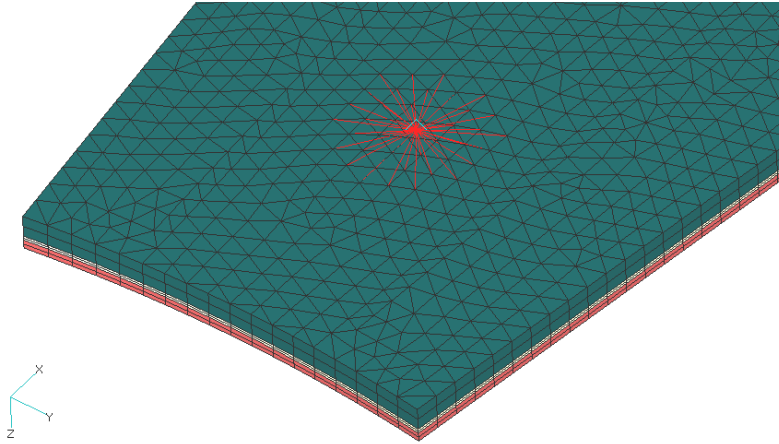


Figure 9: Idealization of a bolted connection in the FE model.

The 3-D FEM is first used to solve the steady-state heat transfer problem with volumetric heat generation in the FPHX chips as presented in Table 2, and edge cooled to 13°C. The steady-state temperature distribution is then used as a load to investigate thermal distortions. Analysis results for three different backplanes are given in Table 3. The temperature difference from the cooled edge to the warmest FPHX chip at the inner radius of the wedge is denoted as ΔT in the table.

Based on performance and costs, it is concluded that a TPG backplane is not needed for the low levels of input heat. On the other hand, run-of-the-mill graphite fiber laminates such as QI M55J produce uncomfortably high ΔT and are therefore rejected. The K13C2U/RS-3C Gr/CE with a ΔT of 5.35°C is selected for the backplane.

We also compare critical stresses in the assembly with nominal design stresses to evaluate whether failure/fracture is likely to occur. Particular concerns are tensile stresses in the brittle silicon sensor and shear stresses in the adhesives. Table 3 shows that these stresses are very comfortably below even conservative design stresses (acceptable design stresses for the silicon detector and epoxy adhesives are assumed 10.0MPa and 13.8MPa, respectively).

Finally, the fundamental frequencies of the wedges with different backplanes is computed and also listed in Table 3. These frequencies are well above the frequency of any significant excitation expected at the site (see Section 2.11) and therefore resonance of the wedge is not a concern.

| Backplane | Thickness | First Mode | ΔT | Thermal Deflection | Silicon Detector | Non-Conductive Epoxy | Conductive Epoxy |
|-------------------|-----------|------------|------------|--------------------|------------------|----------------------|------------------|
| | | | | | σ_{\max} | τ_{\max} | τ_{\max} |
| | mm | Hz | °C | μm | MPa | MPa | MPa |
| TPG Core Laminate | 0.500 | 456 | 2.1 | 24.9 | 1.8 | 1.2 | 0.8 |
| K13C2U Laminate | 0.508 | 367 | 5.4 | 20.6 | 0.6 | 1.0 | 0.7 |
| M55J Laminate | 0.508 | 337 | 13.2 | 7.5 | 1.1 | 1.0 | 0.8 |

Table 3: 3-D wedge trade studies edge cooled at 13°C (all laminates are assumed to be quasi-isotropic).

The temperature contour for a wedge with a K13C2U backplane is depicted in Figure 10 as predicted by the 3-D steady-state FEM simulation. This plot shows that the temperature gradient is rather insignificant in the tangential (ϕ) direction compared to the radial (R) direction. A cross-section of the temperature distribution, at a radius of about $R=0.106\text{m}$ is shown in Figure 11-a followed by the corresponding temperature contour in Figure 11-b. This figure shows that largest temperature drop occurs through the HDI, just below the FPHX chips.

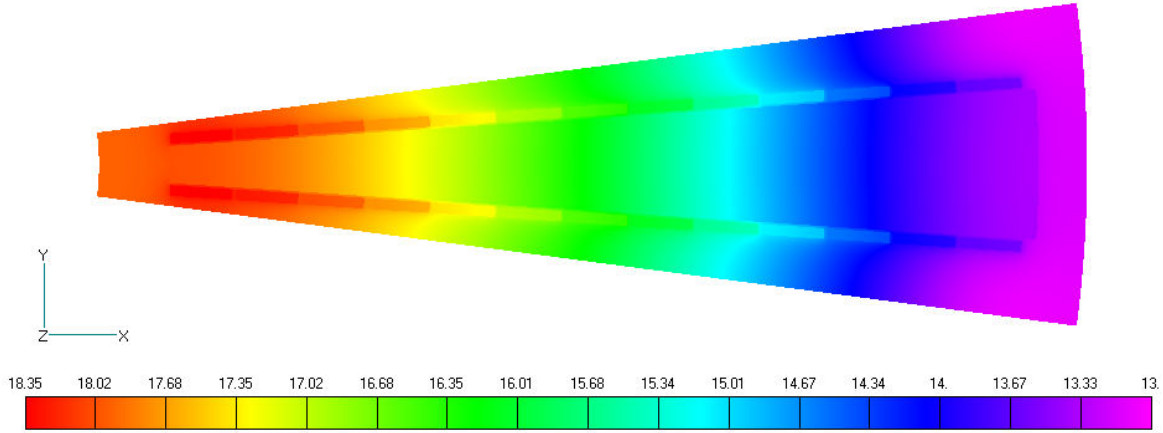


Figure 10: Temperature contour for a wedge with [0/45/90/-45], K13C2U backplane (3-D model, 0.508mm thick backplane).

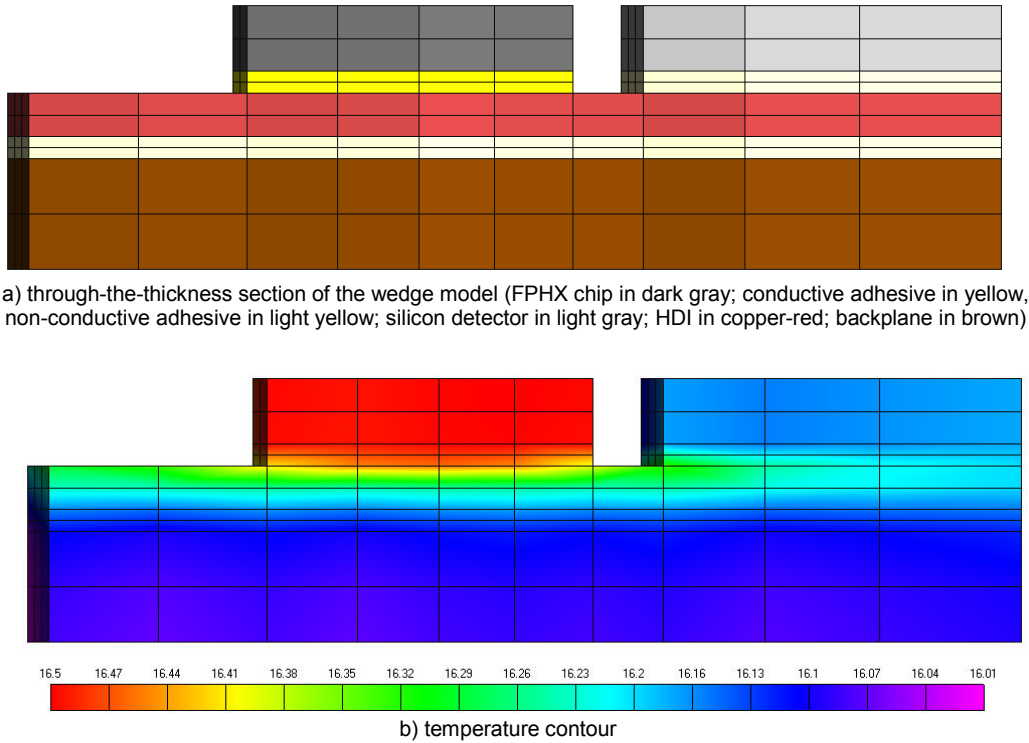


Figure 11: Through-the-thickness temperature contour for a wedge with [0/45/90/-45], K13C2U backplane (3-D model, 0.508mm thick backplane).

Even though the magnitude of this localized drop is quite acceptable, it may be advisable to consider the use of Kapton MT for the HDI (a higher thermal conductivity variety of Kapton, with 3 times the conductivity of the more standard Kapton HN).

The temperature profile along the radial direction of the wedge is shown in Figure 12. This diagram provides a rather useful insight to heat conduction in the wedge. Temperature variation can be approximated with a quadratic function of the radial coordinate R with reasonable accuracy (neglecting the slight temperature variations with ϕ and Z). This simplifies further trade studies and disk-level simulations.

The deformed shape of the wedge under the temperature load is depicted in Figure 13. The wedge is bowing inwards with a maximum thermal distortion of 21 microns in the center of the silicon detector. Figure 14 shows the thermal distortion along the centerline of the silicon detector. If the temperature profile is such that a portion of the wedge is below room temperature and the remaining portion is above room temperature, there is a possibility that the wedge will deform into a full sine wave rather than a half sine wave (e.g., the M55J backplane as reported in Table 3). As a result, thermal distortions might be reduced; however, some of the FPHX chips would have to operate above the room temperature, which is not acceptable according to Section 2.10. For an optimized design, the coolant temperature has to be selected such that (based on the expected ΔT) the warmest FPHX chip would operate just below room temperature.

The thermal distortion for the selected design with a K13C2U backplane is exceeding the dimensional stability requirement described in Section 2.9. In order to improve the bending stiffness of the wedge an increase in the backplane thickness is indicated. By increasing the backplane thickness, not only the flexural stiffness of the wedge will be increased, but the in-plane thermal conduction will be increased as well.

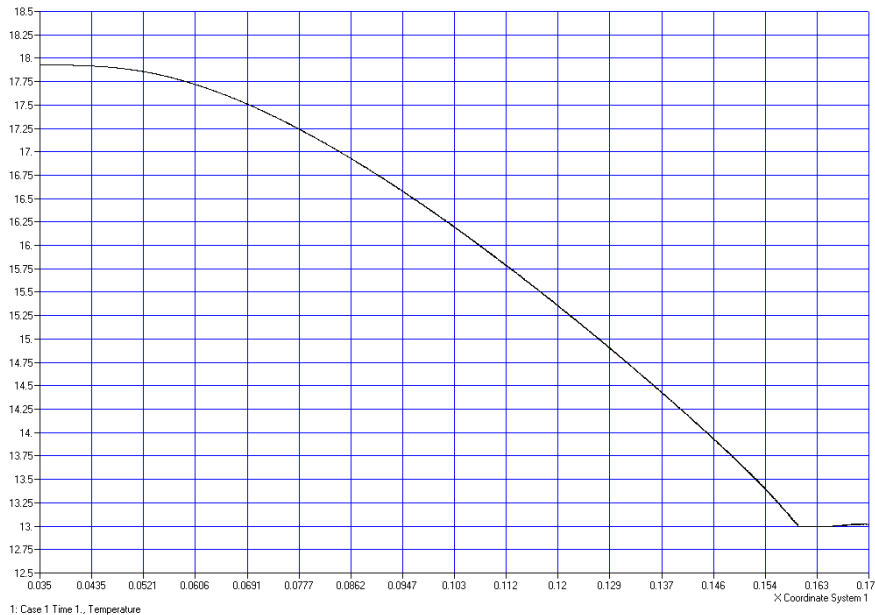


Figure 12: Radial temperature variation of the wedge ([0/45/90/-45], 0.508 K13C2U backplane, 3-D model, temperature along centerline at bottom of backplane).

Results of this detailed 3-D FEM modeling are used as a benchmark to validate a simplified 2-D representation of the wedge. Appendix C compares analysis results obtained from 3-D simulations with that of the 2-D model using laminate plate elements and demonstrates that the 2-D model predicts the wedge response with an acceptable accuracy while substantially reducing the computational time.

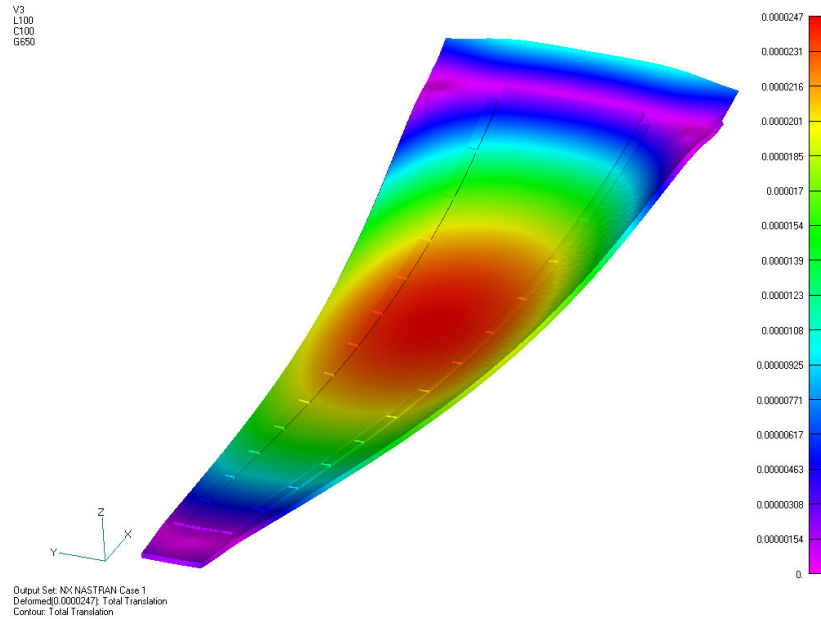


Figure 13: Wedge thermal distortion with [0/45/90/-45], K13C2U backplane (3-D model, edge cooled at 13°C).

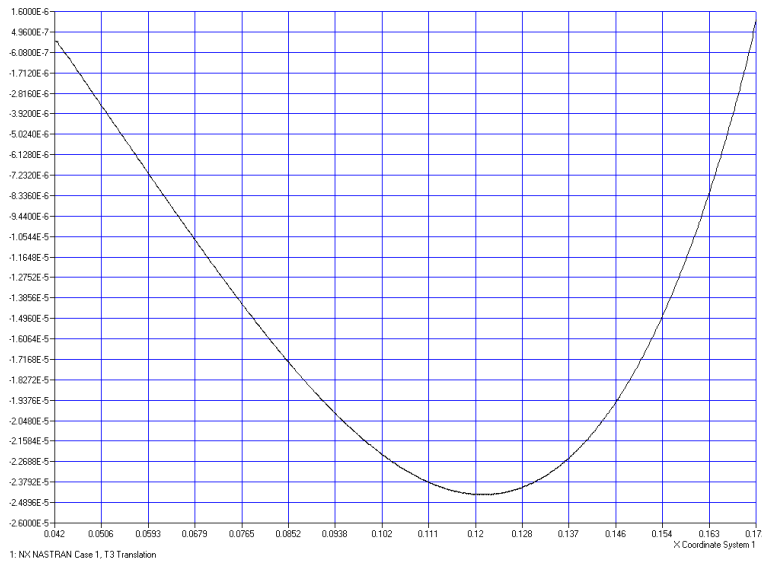


Figure 14: Thermal distortion along the centerline of the silicon detector (for the solution shown in Figure 13).

3.2.2 Backplane thickness and layup

Using the 2-D model, a trade study is performed for different backplane lay-ups and thicknesses to examine whether directional properties of fiber reinforced composites can be tailored to reduce thermal distortion of the wedge. The temperature drops (ΔT) for these layups are obtained using 3-D steady-state heat transfer analysis (see Table 13 in Appendix A for effective thermal conductivities). A best fit quadratic radial temperature variation is then applied to 2-D wedge models with laminate elements. Thermal distortions based on a room temperature of 21.1°C are summarized in Table 4. In this table, quasi-isotropic layups ($[0/45/90/-45]_s$, $[0/45/90/-45]_{2s}$, $[0/\pm 60]_s$, $[0/\pm 60]_{2s}$, $[0_2/45/90_2/-45]_s$) as well as axially biased layups ($[0_2/45/90/-45]_s$, $[40/0/-40/0]_s$, $[40/0/-40/0]_{2s}$) are compared. It is important to note that increased thickness is not desirable from a radiation length perspective. A $[0/\pm 60]_{2s}$ lay-up is selected as a good compromise. It results in a thermal distortion of less than 13 microns, and a ΔT of about 4.3°C.

| Backplane lay-up | Backplane Thickness (mm) | ΔT (°C) | Thermal Distortion (microns) | Natural Frequency (Hz) |
|-----------------------|--------------------------|-----------------|------------------------------|------------------------|
| $[0/45/90/-45]_s$ | 0.508 | 5.35 | 20.19 | 391.43 |
| $[0/45/90/-45]_{2s}$ | 1.016 | 3.63 | 8.30 | 616.58 |
| | | | | |
| $[0/\pm 60]_s$ | 0.381 | 8.11 | 20.18 | 335.26 |
| $[0/\pm 60]_{2s}$ | 0.762 | 4.33 | 12.16 | 503.54 |
| | | | | |
| $[0_2/45/90/-45]_s$ | 0.635 | 4.06 | 18.73 | 474.34 |
| $[0_2/45/90_2/-45]_s$ | 0.762 | 4.33 | 13.95 | 531.61 |
| | | | | |
| $[40/0/-40/0]_s$ | 0.508 | 3.93 | 23.18 | 382.28 |
| $[40/0/-40/0]_{2s}$ | 1.016 | 2.69 | 8.09 | 644.23 |

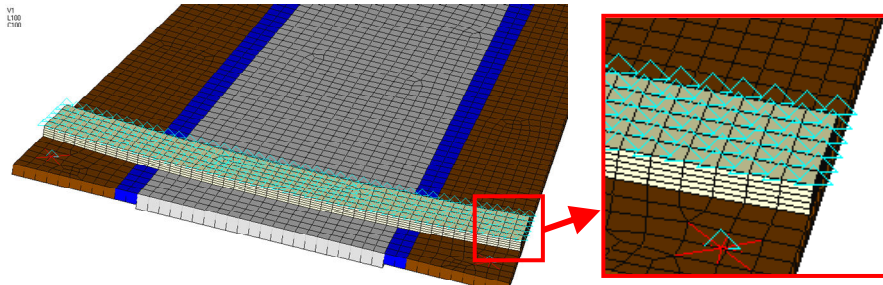
Table 4: K13C2U backplane layup trade studies assuming 13°C edge cooling

3.2.3 Module to station thermal interface

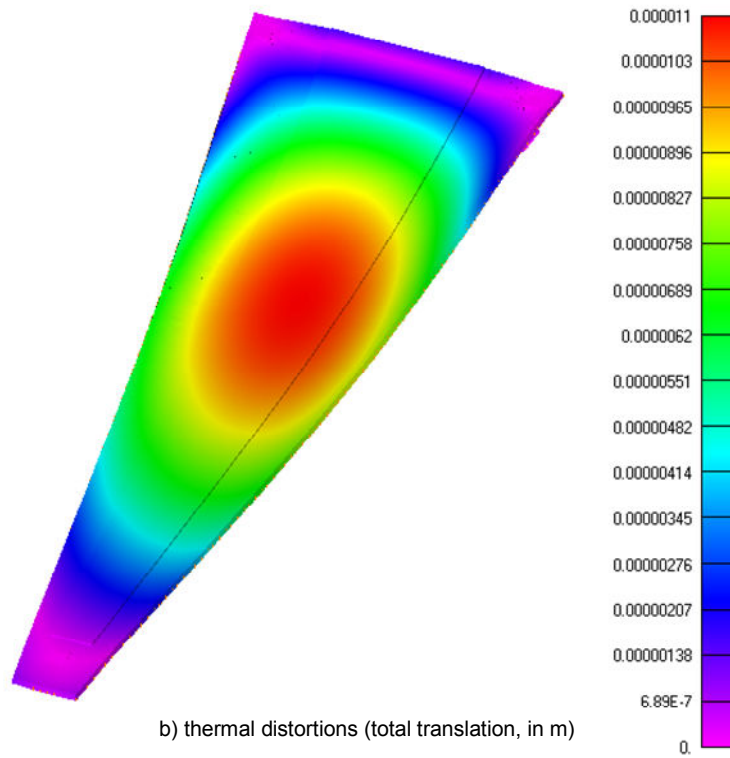
To maintain thermal contact between the wedge backplane and the actively cooled region of the support panel, a layer of thermally conductive silicone is used to glue the backplane to the support panel.

In order to investigate any possible effect of this additional connection, a simplified FE model is prepared. The wedge module is modeled using 2-D laminate elements while the adhesive layer of the conductive silicone is represented using 3-D solid elements as depicted in Figure 15-a. In this model, the backplane is 0.762mm thick with a QI $[0/\pm 60]_{2s}$ layup of K13C2U layers. The silicone adhesive is assumed to have a thickness of 1.0mm (see Appendix A for typical material properties). Structural boundary conditions consist of fixed nodes at the outer surface of the adhesive (shown as small blue triangles in Figure 15-a) and screw connections modeled using spiders of rigid elements. The applied temperature load is a parabolic temperature profile along the radial coordinate R , with edge cooling at 13°C and $\Delta T=4.3^\circ\text{C}$. The reference temperature is set to 21.1°C. Figure 15-b shows the resulting thermal distortion of the wedge (contour plot of total translation). The maximum distortion is 11.0 μm . The thermal distortion of the wedge remains essentially unchanged with the addition of the silicone adhesive compared to the case without the adhesive (shown in Table 4). Therefore, it is concluded that although conductive

silicone has a relatively high CTE, it is compliant enough not to have any significant impact on the thermal distortions.



a) close-up of the silicone adhesive in the model



b) thermal distortions (total translation, in m)

Figure 15: Wedge module with screw connections and silicone bonding ([0/±60]_{2s} K13C2U backplane edge cooled at 13°C)

3.3 Half-disk assembly

A 2-D FE model is prepared for the half disk assembly as depicted in Figure 16-a. In this model, the support panel is a sandwich plate with Aluminum honeycomb core (HEXCEL 3/16-5056-0.0007, 2.0 lb/ft³) 4.76mm thick (3/16"), and symmetric [0/45/90/-45]_s M55J/954-3 composite face-sheets where each layer has a thickness of 0.0635mm (see Appendix A for material properties). On either side of the support panel, twelve wedges are connected to the panel using three screws each. Each support panel is in turn connected at three tabs to the cage. To model

this connection, a set of nodes at the footprint of the screw connections on each tab are fixed in all degrees of freedom using rigid elements.

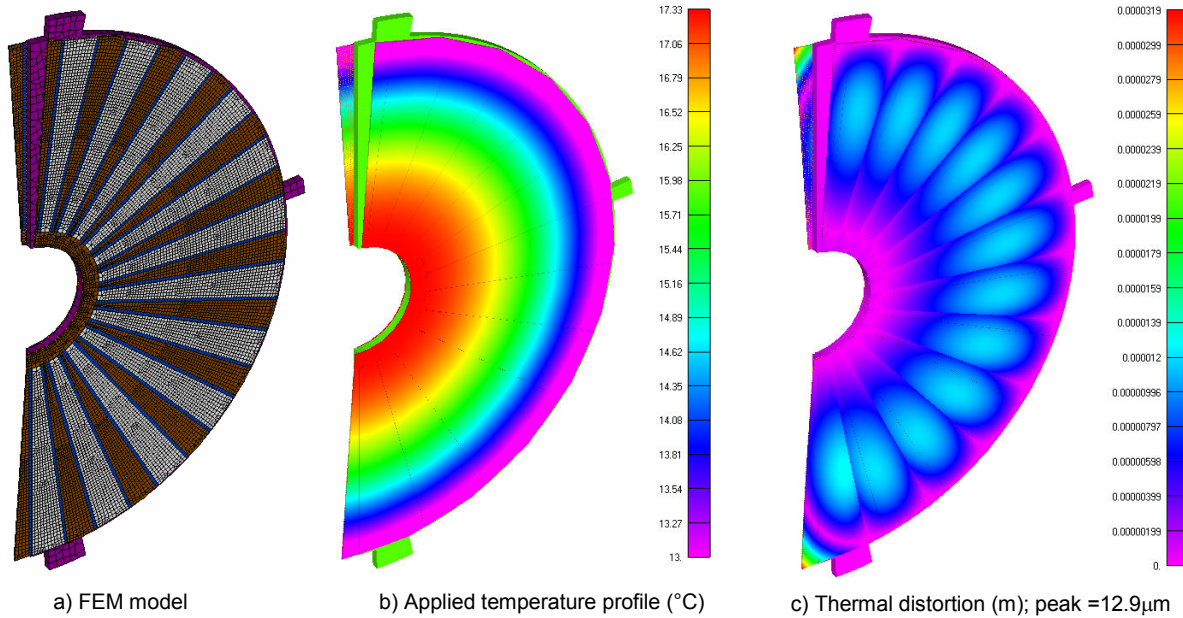


Figure 16: FVTX half-disk assembly ([0/±60]_{2s} K13C2U wedge backplane and edge cooled at 13°C)

Based on the wedge heat transfer studies conducted in Section 3.2, a quadratic temperature variation is applied to the wedges in the half-disk assembly as shown in Figure 16-b to emulate the temperature distribution shown in Figure 12.

The backplane is assumed to have a uniform temperature of 15.9°C equal to the average wedge temperature. The reference room temperature is set to 21.1°C and a thermal distortion analysis is performed. Figure 16-c shows the deformation contour, with maximum amplitude of about 12.9 microns in the active area. In this figure, wedges are bowing inwards, which is consistent with the stand-alone wedge analysis shown in Figure 13. It is important to notice that because of the clamshell design concept of the FVTX cages, two of the wedges (located approximately at 12 and 6 o'clock positions as shown in Figure 16-a) are connected to the support panel only on one side and therefore result in a maximum distortion of 32 microns. This is occurring outside of the active wedge area and only for two of the wedges on each half disk (the maximum thermal distortion in the active area of these two wedges is about 17.4μm). Finally, free vibration analysis of the wedge yields a drum-mode natural frequency of 177 Hz which is well above the goals discussed in Section 2.11.

3.4 Half-Arm Assembly

The FVTX half-arm assembly consists of the structural support shell and the four half-disks mounted into it as depicted in Figure 17-a. This structure is made from a honeycomb sandwich panel with Aluminum core (HEXCEL 3/16-5056-0.0007, 2.0 lb/ft³) and quasi-isotropic [0/45/90/-45]_s Gr/CE (M55J/954-3) 0.254mm thick face-sheets resulting in a total thickness of 5.27mm. The cutouts in the cage design are conceptual and are intended to reduce the structural mass and RL impact. Figure 17-b shows the cage assembly with detector stations installed.

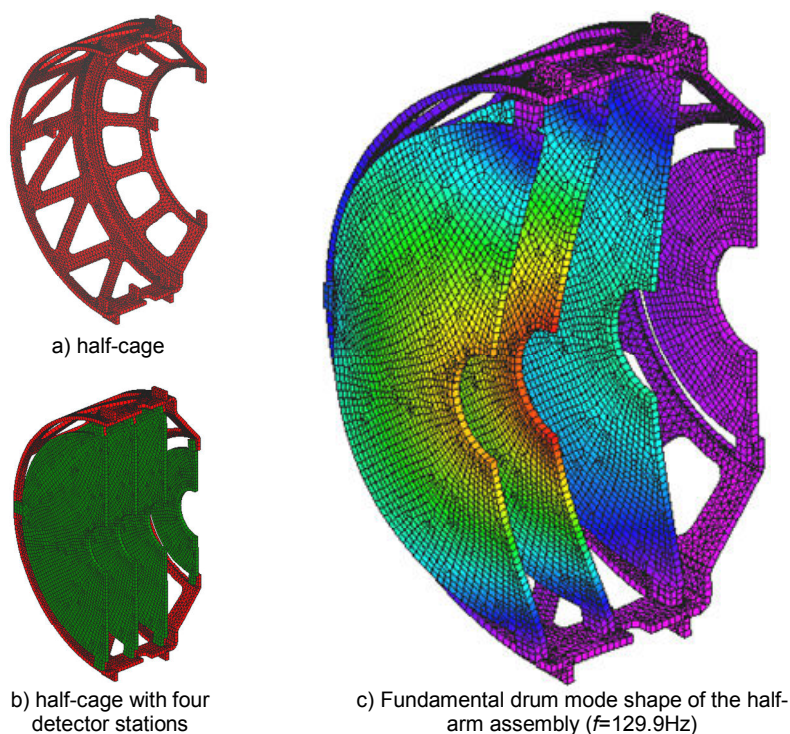


Figure 17: FVTX half-arm assembly.

Since thermal distortion of a single station (disk assembly) was studied in the previous section, here we only focus on the natural frequencies of the half-arm assembly. In the simplified model depicted in Figure 17-b, wedge modules are not shown. Each disk is made of the standard sandwich support panel, and to account for the wedge modules, non-structural mass is tuned to match the natural frequency of the detailed half-disk model (i.e. 177Hz). Since wedge modules are connected to the support panel at three discrete locations only, their contribution to the flexural stiffness of the support panel is small and they primarily act as added non-structural masses. The cage is connected to the VTX space frame through four tabs at the 12 o'clock and 6 o'clock positions. For the simulations presented here, these tabs are connected to fixed supports. This is in effect assuming an infinitely stiff VTX space frame and therefore over-predicting the vibration frequencies of the cage assembly. The fundamental mode is a drum mode of the disks with a frequency of 130Hz as shown in Figure 17-c. The following modes are 140Hz, 145Hz, 208Hz, and 213Hz. Based on this analysis, it is concluded that resonance of the cage assembly is unlikely to be a concern.

4. Preliminary Design Description

4.1 Modular Design Approach

The FVTX is built with three levels of modularity. They are illustrated in Figure 18.

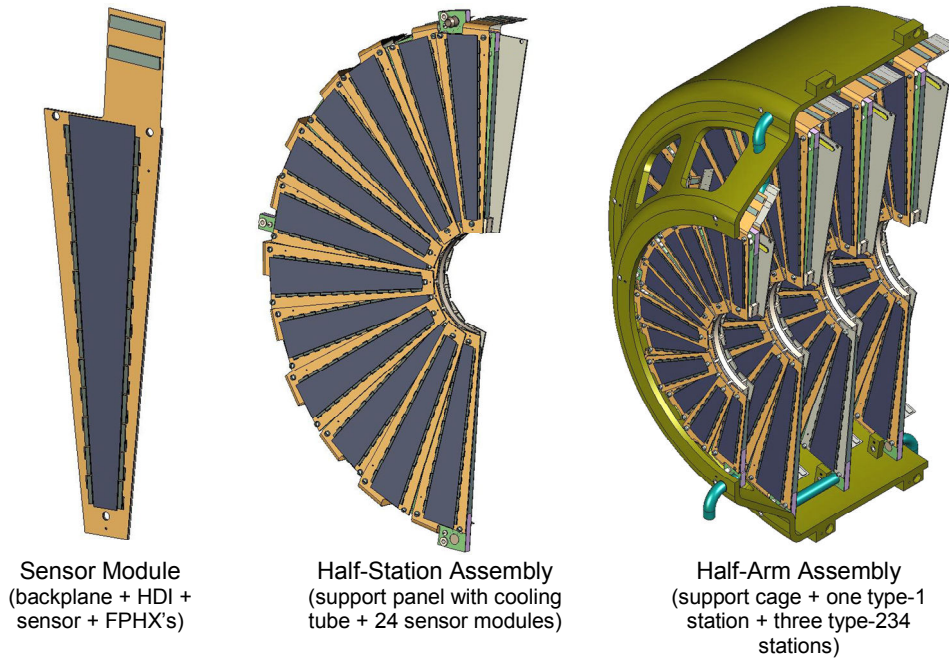


Figure 18: Modular design approach

4.1.1 Sensor modules

The entire FVTX is built from two different sizes of sensor modules (Type 1 and Type 2,3,4, for station 1 and stations 2, 3, or 4, respectively).

Within each type, all modules are exactly identical, with one exception: the HDI tail is bent at 90 degrees, either toward the backplane or toward the sensor, depending on whether the module will be mounted on the upstream or downstream side of the station, respectively (Figure 19). In case the bend in the HDI tail was to be pre-formed during manufacturing of that component, two versions would need to be produced. If, conversely, the tail was simply flexed during integration, all HDI's of each size would be exactly identical to each other.

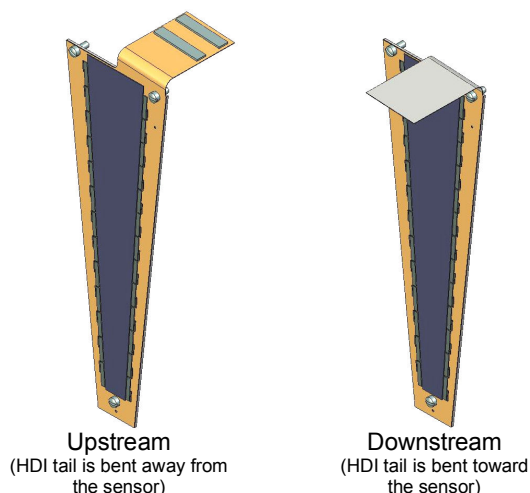


Figure 19: Upstream and downstream variants of the HDI.

4.1.2 Half-stations

The sensor modules are assembled onto three types of support panels to produce three types of half-stations:

- A. Half station 1 (4 ea[‡])
- B. Half station 2 or 4 (8 ea[‡])
- C. Half station 3 (4 ea[‡])

Note that the only difference between half-stations 2/4 (type B) and 3 (type C) is the orientation of the hose barb for interfacing with the coolant hose. The barbs are aligned in the Z direction, but face in opposite directions in type B and type C. This implies that two versions of the large cooling tubes and support panel assemblies will be required.

4.1.3 Half-arm assembly

Three large half-stations (types B and C) and one small half-station (type A) are integrated into a half-cage to produce a half-arm assembly. There are four *identical* half-arm assemblies. They represent the final level of modularity. They are attached to the ends of the VTX support frame before joining the two halves around the beam pipe.

4.2 Sensor Module

The design of the sensor module is illustrated in Figure 20. It is composed of a thermal/structural backplane, to which the HDI, sensor, and FPHX chips are bonded. A complete sensor module for stations 2, 3, or 4 is expected to weigh less than 8.5 grams.

[‡] for the entire FVTX, i.e. two arms, and four half-stations.

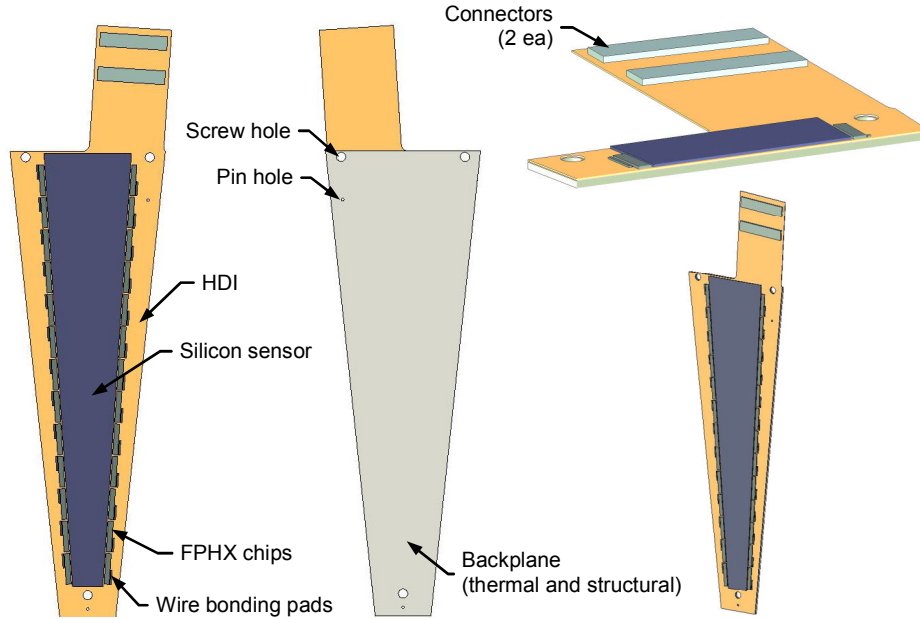


Figure 20: Design of FVTX sensor modules (power/ground connector and decoupling capacitors not shown).

4.2.1 Backplane

The sensor module is built on a flat, constant-thickness graphite fiber composite backplane that serves both as structural support and heat transfer path. As a heat transfer device, it conducts the heat from the FPHX chips to the vicinity of the outer radius, where the cooling tube is integrated into the station support panel.

The backplane is made from 12 layers of K13C2U/RS-3C unidirectional tape. K13C2U is an ultra-high thermal conductivity, pitch-based fiber made by Mitsubishi Chemical. Its thermal conductivity is 620W/mK, more than 60% higher than pure copper, and over 60% of the conductivity of Amoco's K1100, the most conductive (>1000W/mK) fiber commercially available today. RS-3C is a cyanate ester resin that is commonly used in aerospace applications, in part for its very low moisture absorption characteristics, which lead to very high dimensional stability. Based on the trade studies described in Section 3, we have chosen a quasi-isotropic layup $[0/\pm 60]_{2s}$, with a total nominal thickness of 0.76mm.

This resin matrix composite was chosen over carbon-carbon composites and pyrolytic graphite because of its attractive mechanical properties and ease of use, in view of the very low power density of the FVTX sensor module. The heat flux is low enough to make the relatively low through-the-thickness conductivity of a resin-based composite sufficient (the through-the-thickness temperature drop in the backplane is less than 0.5°C, see Figure 11). The use of high-conductivity fiber also makes the in-plane conductivity of the composite (179W/mK or about 47% of that of pure copper) sufficient to keep the radial temperature drop along the module to a very reasonable 4.3°C. And of course the density (radiation length) of the composite is about 5 times lower (17 times higher; 25cm for GFRP compared to 1.4cm for Cu) than that of copper.

The backplanes will be machined from plates of the specified composite. Each backplane features three low-precision through-holes for attachment screws, and two high precision (slip fit,

with close diameter and positional tolerances) pin holes for alignment of the modules to the half-station support panels and to the bonding tools (see Section 4.2.2). A precision slot may be substituted for one of the pin holes to remove the over-constraint, although this may not be necessary given that all components will have to be machined to very close tolerances anyway. This level of precision should be relatively easy to achieve with careful machining on standard CNC mills.

4.2.2 Bond design

Detailed design of the bonds between the backplane, HDI, sensors, and FPHX chips, and detailed specification of the adhesive types are beyond the scope of preliminary design.

Room-temperature-cured epoxies are baselined for all these bonds (elevated temperature cures would produce large post-cure deformations and high stresses).

Our analysis (Section 5) shows that, given the limited temperature difference between assembly (room temperature) and operation, standard rigid epoxies are appropriate (CTE-induced stresses are low). Also, given the low power density of heat dissipation in the modules, regular “non-conductive” (0.2W/mK, typ.) epoxies can be used for all but the FPHX to HDI bonds. For the latter, a 1.2W/mK dielectric but thermally conductive epoxy is baselined and recommended.

The bonds may or may not be full-coverage. Full coverage bonds can be difficult to produce reliably without excessive bleed-out and/or air inclusions. At a minimum, the areas directly below any wire-bonding pads will need to be bonded (to keep them rigid). Away from these areas, the mechanical loading on these structures is limited to gravitational pull, which likely makes partial coverage bonds (Figure 21) viable (although analysis has not been conducted to confirm this; all analyses documented in this report assume full-coverage bonds).

Finally, we need to provide electrical contact between the HDI and the sensors (for application of the bias voltage). However, a full-coverage electrically conductive bond is not required, and not recommended since the strength of electrically conductive adhesive is typically much less than that of structural adhesives. The reliability of this electrical contact is obviously critical. A possible approach that would produce mechanically rigid and stable support for the sensor, but at the same time a reliable electrical contact to the sensor may consist of a hybrid bond: partial coverage structural bond made with a semi-rigid clear epoxy (non-conductive), combined with a few discrete dots of a more flexible (maybe a controlled-volatility silver-loaded silicone, or a plasticized epoxy) electrically conductive adhesive. The higher flexibility of the conductive bond would virtually eliminate the risk of bond failure from accidental loading and/or thermally induced stresses, since the majority of the load would be carried by the more rigid structural bond.

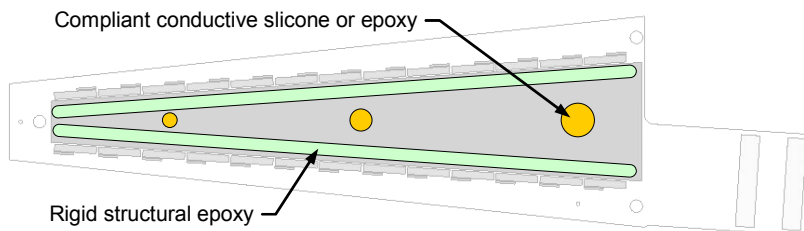


Figure 21: Possible bond pattern between the HDI and the silicon micro-strip detector.

4.2.3 Assembly approach

During assembly of the sensor modules, the silicon strip detector must be aligned to the backplane with micron-level accuracy[§]. The HDI and FPHX chips must also be carefully aligned, but with a precision of the order of tens of microns.

To achieve this, we envision using a set of three precision tools. Each tool would feature a vacuum chuck to cleanly and accurately hold the component to be bonded (Figure 22).

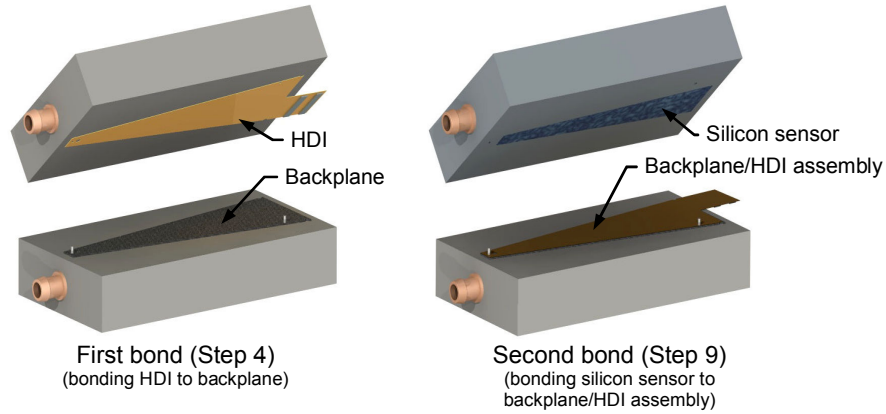


Figure 22: Conceptual illustration of the sensor module assembly process.

The procedure would conceptually consist of the following steps:

1. The backplane is set on a base tool and held in place by a vacuum. The base tool features two precision bores in which dowel pins are temporarily inserted to align the backplane (using the two pin holes in the backplane). Those pins are removed once the vacuum is established
2. The HDI is similarly set, held, and aligned onto a mating tool. The HDI may already be populated with FPHX chips, decoupling capacitors, and connectors (another option may be to bond the FPHX chips onto the HDI at the same time as the sensor, using one common tool). Alignment could be achieved either with removable pins, as is the case of the backplane, or by optical methods.
3. Epoxy adhesive is dispensed onto the backplane (or the HDI) in a controlled manner (perhaps using a robotic dispenser).
4. The tool holding the HDI is flipped and lowered onto the base tool. A kinematic set of alignment features (2 pins in holes and slots, or 3 diamond pins, or 3 ball-in-groove sets) provides precision in-plane alignment of the two tools relative to one-another. Bond thickness control is provided by precision bosses in the tool or the set height of the ball-in-groove sets.
5. The adhesive is allowed to cure at room temperature for several hours.
6. The vacuum is released from the top tool and that tool is removed.

[§] An alternative approach would consist of surveying the fully assembled half-stations, and using the survey data to build look-up tables for use by the track reconstruction software.

7. The silicon sensor is set on a third vacuum chuck/tool. Alignment to this tool is performed optically, by sighting fiducials on the sensor and the tool. That alignment is maintained once the vacuum is established.
8. Beads of structural epoxy and dots of conductive adhesive (Figure 21) are laid on the HDI (or on the sensor) by a robotic dispenser.
9. The tool is flipped and lowered onto the base tool. Alignment and bond thickness control is provided by kinematic sets and/or bosses as in step 4.
10. The adhesives are allowed to cure at room temperature for several hours.
11. The vacuum is released from the top tool and that tool is removed.
12. The vacuum is released from the base tool and the sensor module is removed.

The next steps consist of installing and potting the wire-bonds between the sensor, the FPHX chips, and the HDI.

The detailed design of the tooling and robotic stations required to implement this concept is beyond the scope of this contract.

4.3 Half-Station Sub-Assembly

Twenty-four sensor modules are mounted onto a support panel to produce a half-station (twelve modules on each face of the station) as shown in Figure 23. Each module's active area covers slightly more than a 7.5° azimuthal wedge. The modules on each face are spaced every 15 degrees in azimuth, providing just over 50% coverage from each face. Modules on each face of each station are then staggered in azimuth by 7.5° , to provide full hermetic coverage (at normal incidence) by each individual station.

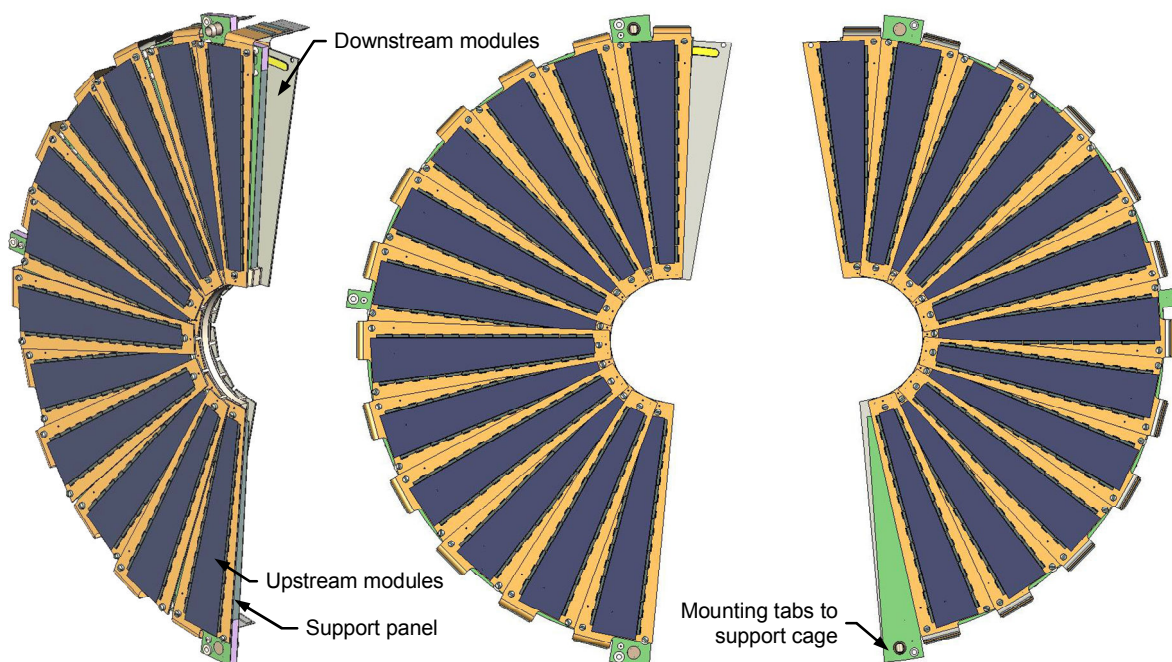


**Figure 23: Preliminary design of FVTX stations 2, 3, and 4;
 Station 1 construction is similar, only smaller.**

Each sensor module is aligned to the support panel using two small-diameter pins, and held in place with three small nylon screws^[21]. To maintain the accuracy of the alignment without relying on friction in the bolted joint, the pins may have to be left in place (light press fit into the support panel). Standard steel pins are of course not an option (even non-magnetic stainless steel has too short a radiation length). We are considering the use of ceramic or glass pins, if they can be found commercially available. Glass fiber/epoxy (G10/FR4) or rigid plastic pins may also be a viable option.

Inserts are bonded in the lightweight sandwich support panel to receive the screws and locating pins. Because it would be extremely challenging to produce a sandwich panel with micron-level flatness and parallelism on both sides, the inserts also serve as standoffs on which the modules are mounted (i.e. the modules are not in direct contact with the faces of the panel).

Because 1) the sensors' active areas cover slightly more than a 7.5° wedge (to achieve a slight overlap), 2) sensor manufacturing requires a sizeable inactive edge around the active area (Figure 6), and 3) additional space is needed on the modules along the sides of the sensors for wire-bonding pads and decoupling capacitors, the backplanes and HDIs have to be made wider than their 15° azimuthal installation pitch on the station support panels. This forces us to stagger the modules in the Z direction (as illustrated in Figure 24, and in contrast with the simpler solution where all modules on each face of a station lie in the same plane).

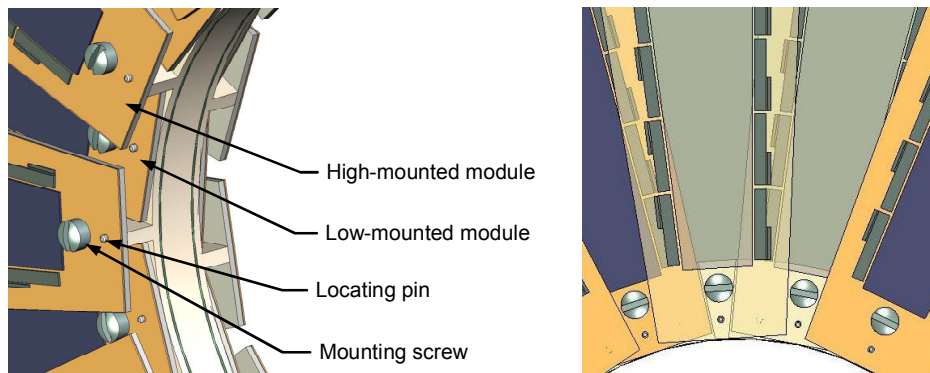


Figure 24: Z-staggering of the sensor modules on each face of a station is required to provide sufficient space for FPHX chips and wire bonding pads.

To achieve this, every other sensor module is mounted on taller standoffs, so that it can overlap its two neighbors. The clearance between the back of the backplane of a high module and the front of the HDI of a neighboring low module is 2.9mm ^[21] to provide sufficient space for the decoupling capacitors and wire bonds (the minimum required clearance is 2.5mm minimum, see Section 2.4).

4.3.1 Support panel construction

The support panel is a lightweight sandwich composite (Figure 25). The main core is a 4.76mm ($3/16''$) thick, very light 5052 aluminum alloy honeycomb (HEXCEL CRIII 3/16-5052-.0007) with a cell size of 4.76mm ($3/16''$) and a foil thickness of 0.018mm ($.0007''$), resulting in an average density of 2 lb/ft^3 (32 kg/m^3), or an average volume occupancy of about 1.2%. Graphite composite face sheets are bonded to either side of this core. Since thermal conductivity is not

required and stiffness requirements are minimal (lightweight payload), a fairly conventional graphite fiber is used (M55J), bound by a cyanate ester matrix such as RS-3C. The layup is a minimum-thickness [0/45/-45/90], 4-ply balanced laminate, with a nominal thickness of 0.254mm (0.01"). These face sheets are bonded to the honeycomb core using a heat-activated epoxy film adhesive.

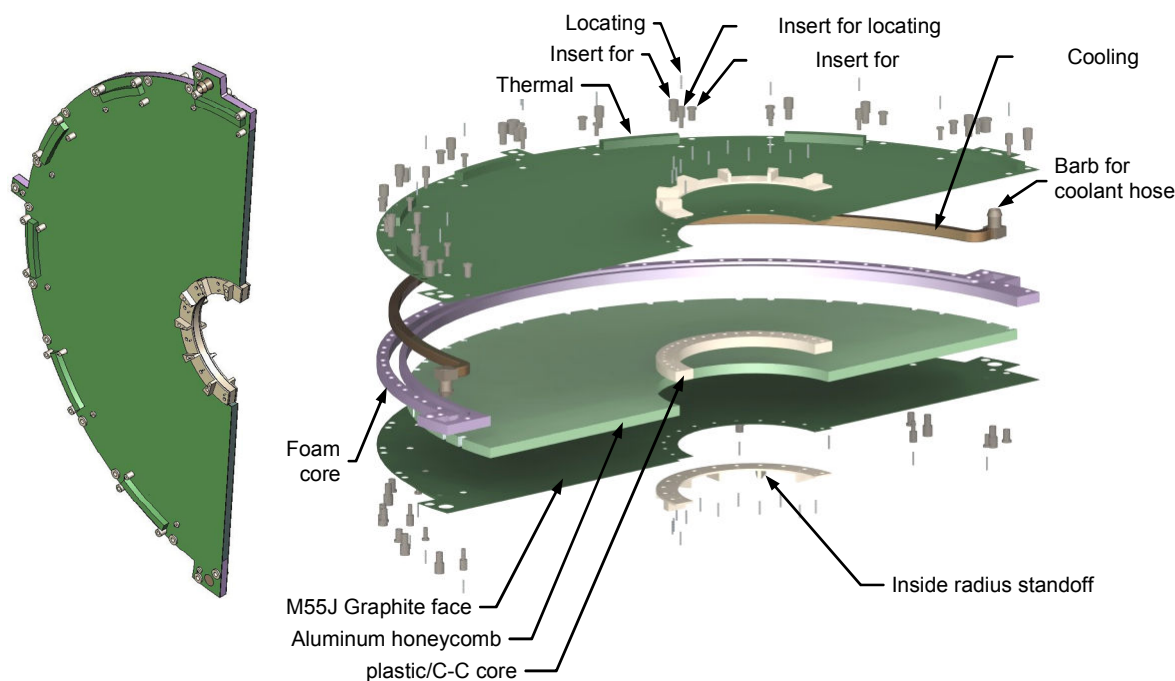


Figure 25: Preliminary design of Support panel for FVTX stations 2, 3, and 4.

The panel is equipped with a large number of inserts to receive the mounting screws for the sensor modules and the alignment pins. Those inserts will be made from either a plastic material (unspecified at this time), or a resin-impregnated, machined carbon-carbon material (available in bulk at low cost from recycled airplane brake disks and pads). The inserts are bonded into holes routed into the main panel, using a room-temperature-cured epoxy. A pair of high precision tools will be used to hold the inserts in position during curing of the adhesive. The positional accuracy of the inserts and their pin holes in the finished panel is thereby made completely independent of the manufacturing accuracy and flatness of the sandwich panel. Another approach that may be considered to achieve the same result is to bond blank inserts into the panel without the use of an alignment tool, then face and drill all these inserts in a single machining operation (per face) on a CNC mill. The final choice of manufacturing approach will be left to the vendor.

As mentioned previously, a cooling tube is embedded near the outer edge of the support panel. This is described in detail in Section 4.5. Because the cooling tube has an extremely thin wall (to keep the total % radiation length as low as possible), a foam core is locally substituted for the honeycomb on both sides of the tube, to help support the tube walls against bulging. Heat transfer bridges are also bonded to the face sheets, outside the panel, to carry the heat from every other high-mounted module to the cooling tube. See Section 4.5 for details.

Finally, three extension tabs are machined in the outer contour of the panel to provide mounting points to the support cage. Plastic or C-C inserts are located in these tabs for the attachment bolts and alignment pins. Two of the tabs also allow routing of the embedded cooling tube to a built-in barbed fitting out of the way of the active area.

A completed half-station support panel (without modules) is expected to weigh about 106 grams.

4.4 Half-Arm Sub-Assembly

The last step of FVTX pre-assembly before integration with the VTX consists of mounting four half-stations into a half support cage to produce a half-arm of the FVTX (Figure 26).

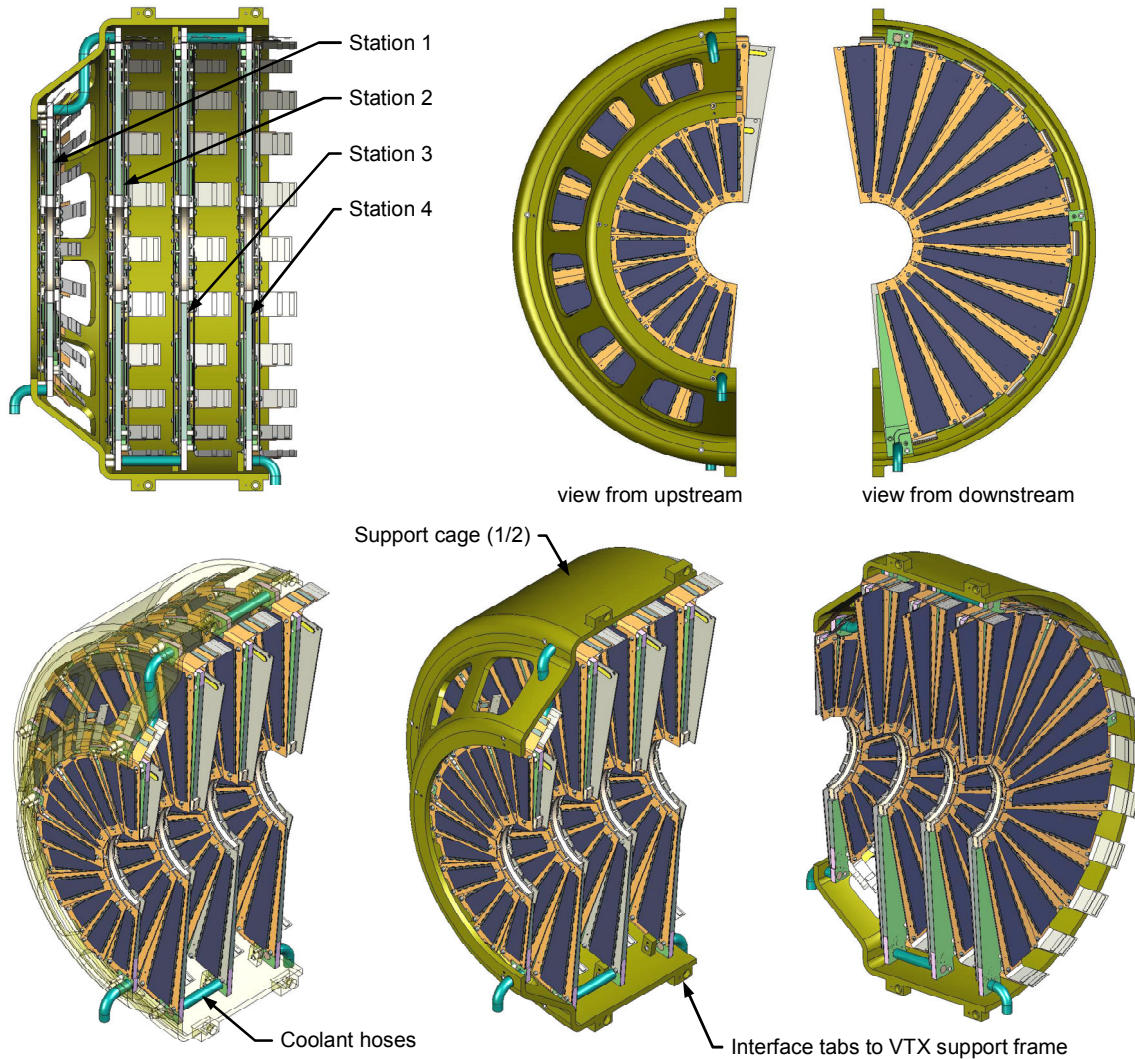


Figure 26: FVTX half-arm sub-assembly.

The cage is currently envisioned as a formed, cylindrical sandwich structure with a relatively complex shape. Manufacturability of this structure has not yet been investigated. The baseline sandwich construction is identical to that used for the station support panels (4.76mm thick, 32kg/m³ aluminum honeycomb with 0.254mm thick M55J/RS-3C graphite composite face sheets).

Each half-shell is equipped with two sets of three mounting tabs (likely made of machined plastic or composite material) to hold half-stations 3 and 4. The other two half-stations are mounted to flat faces at the upstream end of the cage, on plastic (or C-C) standoffs. Alignment of the stations to the cages is provided by precision dowel pins (glass or ceramic). Each station is secured in place by 3 small nylon screws each (one in each tab).

The half-arm assembly is aligned and held on the VTX support frame via four (may later be reduced to three to remove the over-constraint) tabs located near the separation plane between the two halves. Pins and nylon screws are again used to provide alignment and clamping.

4.5 Cooling System

4.5.1 Gas enclosure

The FVTX will reside inside a dry gas enclosure, most likely common to the VTX and the FVTX (the enclosure has not yet been designed, and this activity is outside the scope of this contract). A steady flow of dry nitrogen will be forced into this enclosure to produce a slight over-pressure to prevent moist air from leaking into it, and to provide replacement Nitrogen to compensate for leaks and temperature changes over time. The temperature of this nitrogen supply is a design parameter.

Because the strip-detector layers of the VTX (outer barrels #3 and 4) must operate near 0°C, early design studies had considered operating the gas enclosure at that temperature. However, a thin-walled enclosure at freezing temperature in a large experimental hall in NY state raises serious concerns of condensation and/or frost buildup on the outside of the enclosure. Also, operating the gas enclosure at 0°C suggests that all detector systems within that enclosure should also operate cold. Unfortunately, one of those systems (the interim FVTX, or iFVTX) is not compatible with near-0°C operation. Finally, operating detector systems (which are normally assembled at room temperature) at 0°C requires special care to control the build up of thermal stresses and CTE-induced deformations.

These reasons have led us to baseline operation of the gas enclosure at or near room temperature. All detector systems (VTX, FVTX, and iFVTX) will also be operated near room temperature, with the exception of the VTX strip layers #3 and 4, which will be cooled to about 0°C. Because of the room-temperature gas purge, these two layers will have to be cooled more aggressively, to compensate for additional heat input from the nitrogen and neighboring detectors and structures, via natural convection and radiation. This decision however eliminates any concern of condensation and frost, and allows the rest of the detector system to operate near room-temperature, with improved dimensional stability and reduced thermal stresses.

4.5.2 Active cooling of FVTX stations

During normal operation, waste heat is dissipated in the FPHX chips on every module of the FVTX. This heat must be evacuated from the detector space to maintain the chips at their normal operating temperature. The total power dissipated in the entire VTX (both arms) is moderate, about 111W.

This heat is passively conducted from the FPHX chips, through the HDI, into the backplane, and radially out along the backplane to the outer radius of each station (Figure 27). From there, it travels through an interface material (and, for high-mounted modules, a thermal bridge standoff), then through the face sheet of the support panel and the cooling tube wall, into the coolant.

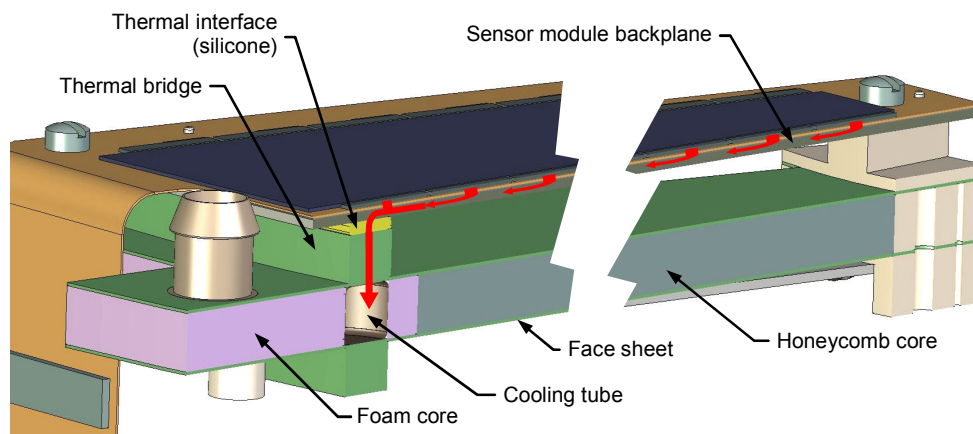


Figure 27: Heat transfer path from the FPHX chips to the coolant.

| Property | Novec HFE 7000 | Water |
|---|--|------------------------|
| Chemical Composition | $C_3F_7OCH_3$ (1-methoxyheptafluoropropane) | H_2O |
| Dynamic Viscosity (centiPoise) | 0.45 | 1 |
| Surface Tension (dyne/cm) | 12 | 73 |
| Density (kg/m^3) | 1400 | 1000 |
| Radiation Length (cm) | 25.2 | 36.1 |
| Specific Heat ($J/kg/^\circ C$) | 1300 | 4187 |
| Thermal conductivity ($W/m/^\circ C$) | 0.075 | ~ 0.6 |
| Freezing point ($^\circ C$, at 1 atm) | -123 | 0 |
| Boiling point ($^\circ C$, at 1 atm) | 34 | 100 |
| Toxicity | Very low | None |
| Flammable | No | No |
| Ozone Depletion Potential | None | None |
| Non-volatile residue | <1 ppm | Variable |
| Electrically conductive | No | Depends on ion content |

Table 5: Key properties of 3M Novec HFE 7000, compared to those of water (at room temperature).

Given the relatively low power to be removed, a single phase, forced convective cooling loop is sufficient. The coolant we have tentatively selected is Novec™ HFE-7000, a member of a new generation of hydrofluoroethers (HFE's) produced by the 3M Company. It is a replacement for earlier CFCs, whose environmental impact is unacceptable. Even though it is inferior to water as a coolant (much lower specific heat and thermal conductivity, see Table 5), it presents several attractive qualities:

- non-conductive (many order of magnitude lower resistivity than CFC's, but still higher than the best available DI water^[32])
- non-corrosive to metals and compatible with rigid plastics and elastomers (with low plasticizer content)^[32]
- low viscosity (less than half that of water)
- very low toxicity
- very low known environmental impact (zero ozone depletion potential)
- evaporates extremely quickly
- very low freezing point
- unregulated, mostly harmless chemical

These qualities make it attractive for this complex system, with numerous flexible hose connections (particularly true of the VTX) in an inaccessible space, because it makes small leaks a very minor issue. Even liquid HFE-7000 flowing directly onto microelectronics should not have any negative impact (although little historical data is available to confirm this^[32]), as it is dielectric and evaporates quickly, leaving no residue. Leakage is only an issue in terms of the loss of fluid, and the resulting vapors. Any halogen leak detector can be used to detect leaks^[32].

Among the disadvantages of HFE-7000 are its relatively high cost, and its propensity to leak easily because of its low surface tension.

Also, because of the presence of hydrogen in its molecule, HFE-7000 (and other variations in the same Novec™ family) is known to leach plasticizers out of polymers^[32]. For that reason, care must be taken that only rigid plastics, or polymers with low or no plasticizer content come in regular contact with the fluid. The main negative result of plasticizer leaching is contamination of the coolant, and possible clogging of filters^[32].

3M does not maintain a list of compatible materials, because compatibility with HFEs must be treated on a case by case basis. Slight variations in formulation from one polymer supplier to another (such as the addition of plasticizers) can make all the difference. Specific information about formulations from specific vendors that have already been tested is available from 3M. The company also offers testing of any questionable material at no charge.

Rigid plastics (such as polyethylene, Nylon, PVC, etc) and rigid epoxies are compatible with Novec™ fluids. Rubbery polymers should be treated as suspect and tested. Silicones are only compatible if completely free of plasticizers. Some specific types have already been approved by 3M. Also, plasticized adhesives (such as compliant epoxies) may be problematic and should be tested (although at this point we do not see the need for flexible adhesives in the FVTX).

4.5.3 Cooling tube

Figure 28 and Figure 29 show some details of the cooling tube arrangement. We are baselining the use of a thin-walled nickel/copper composite tube, produced by electro-deposition of nickel and copper onto a sacrificial aluminum mandrel. The mandrel is pre-formed to match the desired finished shape and later chemically dissolved, leaving a tubular structure with a wall thickness that can easily reach down into the 50 micron range, and be completely leak-proof. We have a small contract in place with the vendor of this technology to attempt to produce a prototype tube. Results are expected within about 4 weeks after publication of this report.

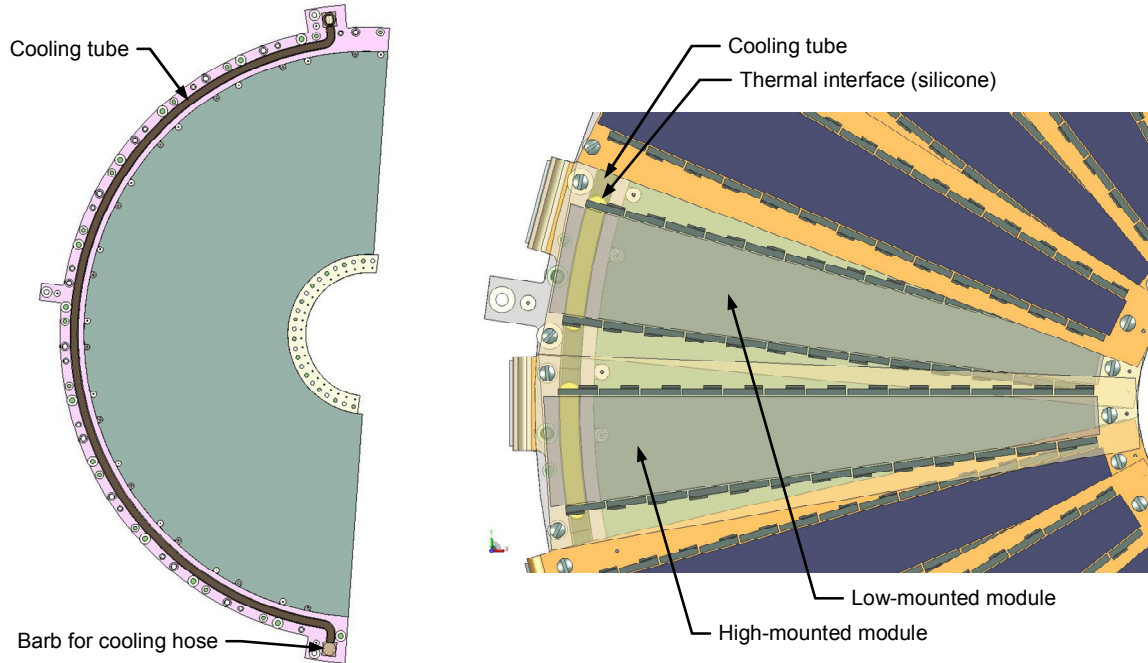


Figure 28: Cooling features of FVTX stations 2, 3, 4.

Barbed fittings are attached to the ends of the tube and embedded in the support panel together with the tube itself. The fittings could be made from metal (perhaps titanium), and welded, brazed, or soldered to the ends of the tube. Alternatively, a plastic fitting could be used, which would be bonded to the tube with an epoxy.

In case of difficulties with the manufacturing of the nickel tubes, a fall-back option may be to use a thin-walled, thermoformed peek tubing technology developed by Fermi Labs for the D-Zero Run2B detectors. This tubing also has very thin wall (0.1mm) and could be a direct substitute for its nickel counterpart. Contacts have been established with FNAL for possible transfer of this technology.

4.5.4 Module to panel thermal bridge

One of the more difficult problems with this design (removable sensor modules) is to insure reliable and predictable thermal contact between the back of the sensor modules and the support panel, in the area of the cooling tube.

We considered the use of heat-transfer grease, but the combination of a relatively thin and delicate module, and the lack of a strong clamping mechanism (the screws are some distance away from the heat transfer area) led us to doubt the reliability of this approach (greases typically require at least 10psi of contact pressure to work reliably). We did in fact analyze the effect of such pressure on the module, and the resulting deformations are large ($\sim 70\mu\text{m}$ bow). Because of this, we cannot recommend the use of grease based on analysis alone. If prototypes can be built and successfully tested with a grease interface, this option could again be considered.

Our baseline design makes use of a cured, flexible silicone bond between the module and the panel. This bond is nominally 1 mm thick to allow for relatively easy separation of a failed

module by splitting the bond with a sharp blade. This thick joint leads to a substantial, yet acceptable temperature drop (about 2.4°C).

For low-mounted modules, the silicone bead is applied between the back of the module backplane and the face-sheet of the support panel. Since they are mounted 3.94mm further away from the panel, high-mounted modules are coupled to a heat transfer block that is bonded to the face sheet with a rigid, thermally conductive epoxy (Figure 29). The gap between that block and the back of the module backplane is then filled with 1 mm of conductive silicone. The block is made from a low-density, high thermal conductivity material. A resin-based graphite composite with mostly unidirectional fibers (along Z), or a resin-impregnated C-C material are good candidates.

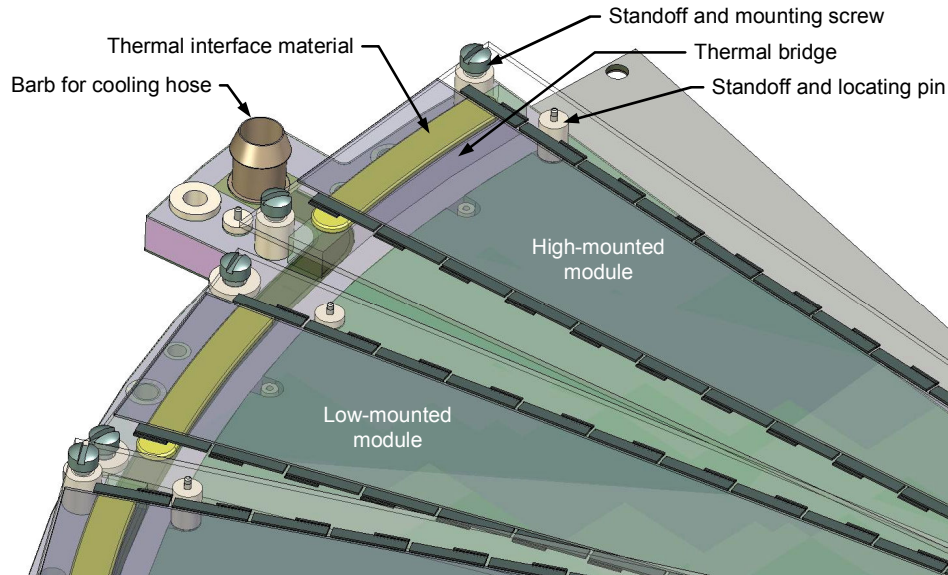


Figure 29: Cooling features of FVTX stations 2, 3, 4
 (HDI's hidden and modules made transparent for clarity).

4.5.5 Cooling circuit

Because the dimensions of our cooling tubes are driven by the thickness of the core of the support panels, and because the selection of a coolant flow velocity is driven by the need to achieve strongly turbulent flow (see Section 5.1), the mass flow rate of coolant in each half-station is relatively high. This, coupled with the relatively low power dissipation, leads to an almost negligible ($\sim 0.3^{\circ}\text{C}$) bulk temperature increase between the inlet and the outlet of any half-station. The pressure drop per half-station is also a very small: 1000Pa (0.15psi). Based on this, and to simplify the cooling circuit, all four half-stations within a half-arm assembly are connected in series. The coolant enters an inlet on half-station 4, then goes from the outlet of half-station 4 to the inlet of half-station 3, and so on, as shown in Figure 31 (and this could of course be reversed). Also, the two half-stations of each arm could be piped in series if desired. This detail has not been decided at time of writing, at least partly because it has more to do with the design of the refrigeration and circulation system, which is outside the scope of this work.

The connections from the refrigeration system to the half-arm assemblies, and between stations are implemented with flexible silicone tubing. As mentioned in Section 4.5.2, care will need to

be exercised to select a silicone formulation that is fully compatible with the Novec™ coolant. At least one type of silicone tubing, available from Cole-Parmer, has already been successfully tested by 3M^[32].

Note that, even though silicone rubber is generally considered a poor performer in high-radiation applications, the expected radiation dose in this application is so low that, based on available data, we don't expect any difficulties (see Section 5.3 for details).

Connections between the silicone rubber hoses and the stations are made with single-barb fittings, as recommended by 3M for HFE fluids. Clamps will be required to secure the tubing onto the fittings. Exact clamp selection is beyond the scope of this work, but various nylon clamps are commercially available for this purpose.

5. Preliminary Design: Performance Predictions

5.1 Cooling System

Cooling of the FVTX is based on a single phase flow of liquid coolant. Specifics of the coolant are provided in Section 4.5.2.

5.1.1 Flow rate of coolant

Liquid flow in pipes occurs in two distinct regimes, depending on the mean flow velocity in the pipe. In laminar flow, pressure drops are low, but heat transfer from the pipe walls to the fluid is inefficient as there is no mixing within the fluid flow. Without mixing, heat transfer is controlled primarily by the conduction properties of the fluid. Because HFE-7000 has very low thermal conductivity (0.075W/mK, or 8 times lower than water, and more than 10 times lower than the through-the-thickness conductivity of the face sheet of the support panel, for example, see Table 5), laminar flow is not an appropriate regime for a cooling system using this fluid.

In contrast, turbulent flow is characterized by strong mixing in the fluid (and a correspondingly higher pressure drop). In that regime, heat is carried into the bulk of the fluid predominantly by turbulence, making the thermal conductivity of the fluid largely irrelevant. Fortunately, the viscosity of HFE-7000 is very low (its dynamic viscosity is less than half that of water), so the flow velocity required to achieve turbulent regime and the resulting pressure drops are both low.

The key indicator of flow regime is the Reynolds (Re) number, which essentially compares inertial stresses in the flow to viscous stresses, and characterizes instability in the flow. It is formulated as

$$\text{Re} = \frac{VD_h}{\mu}, \quad (1)$$

where D_h is the hydraulic diameter of the pipe (which is equal to the diameter for a round cross-section, or the width for a square cross-section), and μ is the dynamic viscosity of the fluid.

It has been established experimentally that the flow in a pipe transitions from laminar (at low Re) to turbulent (high Re) at values of the Reynolds number around 2000 to 3000 (it is not a completely abrupt transition). In this design, we arbitrarily decided to set the design Reynolds number to about 10,000, to ensure a well-established, strongly turbulent regime. For a square

cooling channel cross-section measuring 4.66mm (support panel core thickness minus two times the expected 50µm wall thickness of the tube), and Novec HFE-7000 near room temperature (we have used room temperature properties as an approximation), rounding the mass flow rate to 20g/sec results in a mean flow velocity of 0.66m/s, a volumetric flow rate of 14mL/s (14 gallons/hour), and a Reynolds number of about 9,600.

5.1.2 Cooling tube to bulk fluid temperature drop

Experimentally established, semi-empirical correlations are routinely used to estimate the convective heat transfer coefficient (h) between bulk fluid and tube wall. These correlations establish relationships between three non-dimensional numbers: the Reynolds (Re) number (a measure of turbulence), the Prandtl (Pr) number of the fluid (a material property of the coolant, that compares the viscous effects to thermal diffusivity), and the Nusselt (Nu) number, which compares convective to conductive heat transfer.

The Prandtl number is expressed as

$$Pr = \frac{\mu c_p}{k}, \quad (2)$$

where μ is the dynamic viscosity of the fluid, c_p its specific heat, and k its thermal conductivity. The Prandtl number is a material property of the fluid. For HFE-700, using room-temperature properties listed in Table 5, the Prandtl number is found to be about 7.8.

We use a correlation developed by Sleicher and Rouse^[36] (as reported by Kays and Crawford^[35]), which is applicable to turbulent flow with $10^4 < Re < 10^6$ and $10^{-1} < Pr < 10^4$. Strictly speaking, this correlation applies to pipes with a uniform heat flux into the fluid around the entire wall. In our case, the heat flux is concentrated on the +Z and -Z faces of the cooling tube, but the correlation should still provide a good approximation. It is formulated as:

$$Nu \approx 5 + 0.015 Re^{\left(0.88 - \frac{0.24}{4 + Pr}\right)} Pr^{(0.333 + 0.5e^{-0.6 Pr})} \quad (3)$$

Substituting the Prandtl number of HFE-7000, and the Reynolds number from Section 5.1.1, the Nusselt number is about

$$Nu = \frac{h D_h}{k} \approx 84. \quad (4)$$

Substituting the values of the hydraulic diameter D_h (Section 5.1.1) and the fluid thermal conductivity k (Table 5), the wall heat transfer coefficient is computed as about 1355W/(m²°C).

Assuming – as noted earlier – that only the two faces of the cooling tube in contact with the support panel face sheets carry any heat into the coolant, the average heat flux is about 1498W/m² for half-station 1 and 1770W/m² for half-stations 2 to 4, resulting in a tube wall to bulk fluid temperature drop of about 1.1°C for station 1, and 1.3°C for stations 2 to 4. It should be clear that these are fairly rough estimates, and that testing of prototype assemblies is the most expedient way to refine those estimates.

5.1.3 Temperature drops from tube wall to backplane

In addition to the wall-to-fluid temperature drop, a number of additional drops will occur between the back of the sensor module backplane (where the temperature boundary condition is

applied in the FE models) and the cooling tube. These small drops can be estimated based on the expected geometry and thermal conductivities of the material involved. Figure 30 illustrates this, for a high-mounted module, assuming a coolant temperature of 10°C.

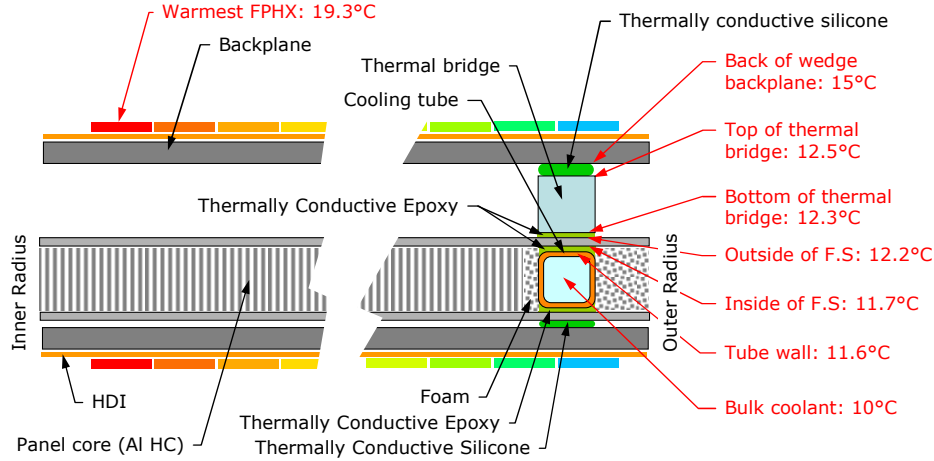


Figure 30: Typical temperature distribution from coolant to FPHX chips.

5.1.4 Pressure drop

Semi-empirical correlations are also routinely used to estimate the pressure drop along a length of pipe as a function of flow rate and fluid properties. The pressure drop in a smooth, straight pipe is often normalized by defining a “friction coefficient” (also known as the Darcy-Weisbach friction factor), f , according to the equation:

$$\Delta p = f \frac{L}{D_h} \frac{\rho V^2}{2}, \quad (5)$$

where L is the length of the pipe, Δp the pressure drop, ρ the density of the fluid, and V the mean flow velocity.

The friction coefficient can then be experimentally correlated to the Reynolds number. As is the case for the wall coefficient, different correlations apply in laminar and turbulent regimes. For turbulent flow with $10,000 < \text{Re} < 50,000$, the widely used Blasius correlation^[35] is formulated as:

$$f \approx \frac{0.312}{\text{Re}^{0.25}}. \quad (6)$$

Substituting values for this application, and neglecting the very shallow curvature of the cooling tube, the pressure drop along the smooth portion of cooling tube for a large (Type B or C) half-station is estimated as 990 Pa (0.15psi). For a small (Type A) station, the same drop is about 540 Pa (0.08psi).

To estimate the pressure drops along the entire circuit (as shown in Figure 31), additional losses must be accounted for at any sharp bends in the flow, for example. Experimental values of *equivalent length of pipe* $(L/D)_{eq}$ are available in the literature^[34] for these discrete effects. With this definition, the total pressure drop in the entire circuit is given by

$$\Delta p = f \left(\frac{L}{D_h} + \sum_i \left(\frac{L}{D} \right)_{eq,i} \right) \frac{\rho V^2}{2}. \quad (7)$$

Neglecting any changes in cross section (such as at the transitions between a flexible hose and a fitting, and from a fitting to the cooling tube proper), accounting for a total length of hose of about 269mm, and for a total of 20 ninety degree bends with a $(L/D)_{eq}$ of 40 each (the mean of two values reported in [34] for different types of elbows), the total pressure drop from the inlet to the outlet of a half-arm subsystem is *estimated* at 11.7kPa (1.7psi).

Figure 31 shows the resulting estimates of temperatures and pressures at key points along the cooling circuit and on the sensor modules (making use of results presented in the next section for the temperature drops along the sensor module, and assuming an inlet gage pressure of 5psi and inlet temperature of 8°C).

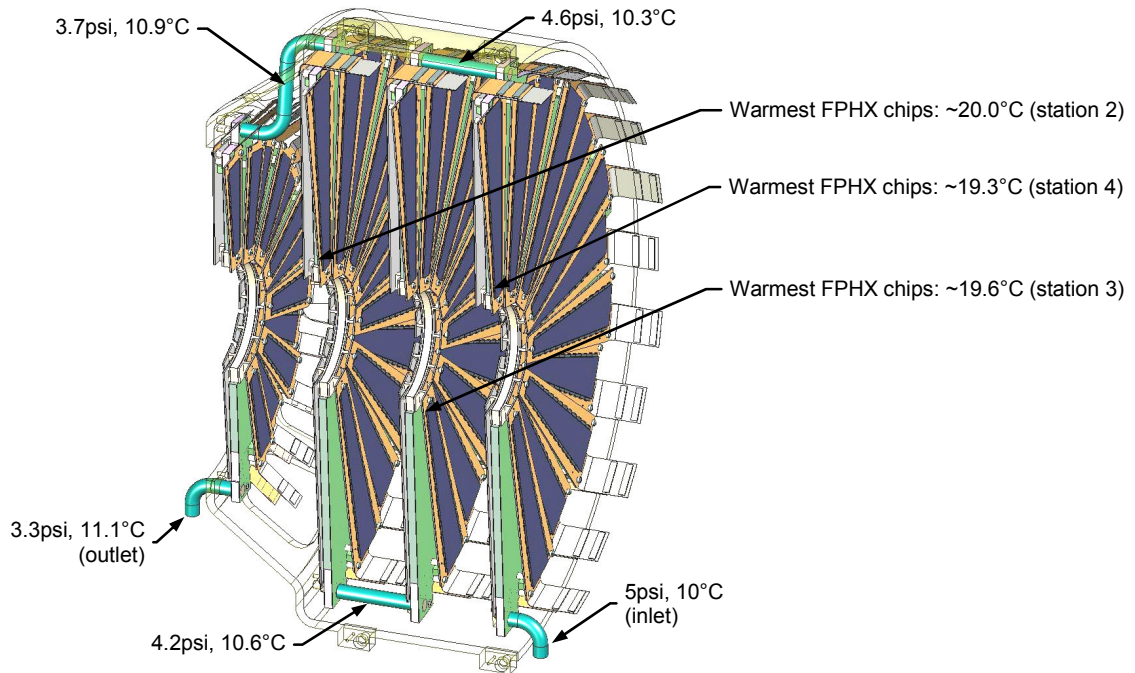


Figure 31: FVTX half-arm cooling system configuration and expected pressures (gage) and temperatures.

5.1.5 Effect of natural convection into dry gas

Since the sensor modules are – in average - slightly cooler than the room temperature dry Nitrogen, natural convective heat transfer will produce an additional heat load into the modules. The exact evaluation of this type of heat transfer is an extremely difficult problem, requiring computational fluid dynamics simulations far beyond the scope of this work. Instead, rough approximations can again be obtained from semi-empirical correlations available in the literature. Those approximations are fairly involved and will not be described here.

Using 17.5°C as the typical (mean) temperature of a module, and 170mm as the vertical extent of the heat-transfer area, one estimates a free-convection heat transfer coefficient of about 3W/(m²°C). Applying this heat transfer coefficient to one face of the module (the other face is

assumed to be too close to the panel for sufficient natural convection flow to develop), one estimates that convective heat transfer from the surrounding gas may account for an additional heat load of the order of 1W per station (with room-temperature N₂ at 21°C).

This represents about a 13% increase from the total heat dissipated in the FPHX chips. Assuming linearity, that increase in power may be expected to cause about a 13% increase in all temperature drops, and a total increase in the temperature of the warmest FPHX chips of the order of 1.6°C. This small increase is likely within the error band of the predictions presented in the report and can therefore be considered negligible.

Of course, the temperature of the nitrogen supply could be adjusted to more closely match the mean temperature of the module, reducing this effect to an arbitrarily small value, or even inverting it (and helping the liquid cooling system). Heat transfer tests of prototype modules are recommended in order to refine the temperature drop predictions beyond what is achievable from simple analysis (see Section 6.2).

5.2 Radiation Length Percentage

In an ideal high-energy particle detector, all interactions would occur in the active volume of the silicon sensors and all interactions would be directly detected. Clearly, this cannot be achieved in practice: cooling and supports require finite amounts of materials. The percent of a radiation length (RL%) of various components used in the cooling and structural support of the sensors is a good indicator of the number of undetected secondary interactions in a particle detector. This is easily estimated based on the thickness and material of the various components, and the radiation lengths of those materials (the thickness of material required to reduce the energy in a normal-incidence beam by a factor 1/e). This material property is available for many common materials (see, for example [10]), but can be difficult to find for more unusual, specialty materials and composites. Table 6 lists the radiation length of various materials used in the estimates. Where a reference is not shown, the numbers used are from previous experience, or - in some cases - best guesses.

| Material | Use | Radiation Length (X0/ ρ , cm) |
|---|--|--|
| Silicon | Sensor, FPHX chips | 9.36 ^[10] |
| Non-conductive epoxy | Sensor to HDI, HDI layer-to-layer, HDI to back-plane, and support panel face sheet to core bonds | 30 |
| Thermally conductive epoxy | FPHX to HDI, and thermal bridge to support panel bond | 10 |
| Kapton | HDI dielectric layers | 28.6 ^[10] |
| Copper | HDI conductive layers | 1.43 ^[10] |
| Kapton/adhesive/copper laminate (based on RL of Kapton, Copper, and adhesive as shown above, and the layup defined in Figure 7) | HDI | 8.56 |
| Resin-based graphite fiber composite | Module back-plane, support panel face sheet | 25 |
| Thermally conductive silicone | Module to support panel thermal interface | 10 |
| Resin impregnated carbon-carbon composite | Thermal bridge for high-mounted modules | 23 |
| Thermo-plastic | Support panel inserts (could also be made from carbon-carbon, at a slight RL penalty) | 35 |
| Aluminum Honeycomb core (2 lb/ft ³ , or 1.194% volume occupancy) | Support panel core, cage core | 741.4 ^[based on 10] |
| Novec HFE-7000 (C ₃ F ₇ OCH ₃) | Cooling fluid | 25.2 ^[based on formulation] |

Table 6: Assumed radiation lengths FVTX materials, as used to arrive at the RL% listed in this section.

Using the numbers from Table 6, different estimates can be calculated. Note that these estimates assume normal incidence (for simplification), do not include smaller items such as locating pins or decoupling capacitors, for example, and are approximations based on simplification in geometry.

First, an *area-averaged* RL contribution can be calculated for an FVTX station. This was performed for stations type B/C (#2, 3, or 4), and the results are summarized in Figure 32. Each contribution in that chart is calculated as if the entire amount of material used for the specific item was uniformly spread across the entire *active area* of the station. The total area-averaged RL contribution of each station is estimated at about 2.41%. Note that the largest contributions in that sense are the backplane (relatively thick), the HDI (contains copper), and fortunately, the sensor itself.

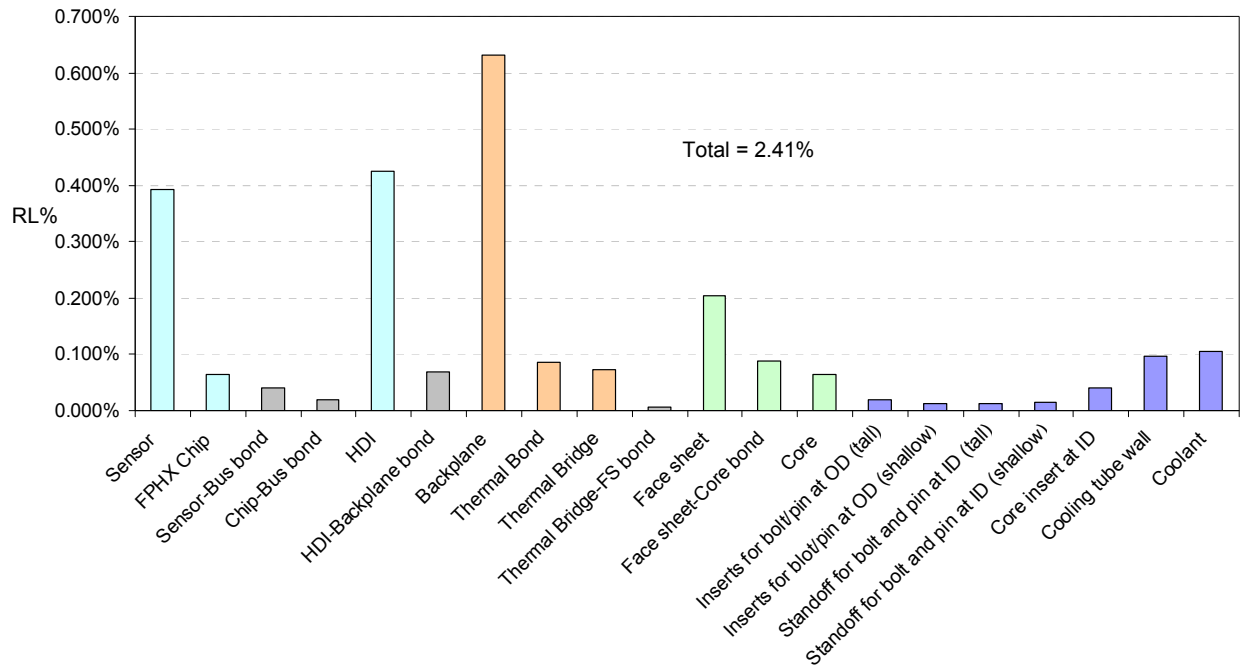


Figure 32: Distribution of individual contributions to area-averaged (normal incidence, normalized to active area) radiation length of FVTX station 2, 3, or 4.

Even though the area-averaged RL contributions are useful global measures of the effects of non-detector materials used in the support and cooling system, extremes in local concentrations of denser materials are also of interest. Figure 33 and Table 7 present such estimates for several representative locations around a station. Note that most the highest values in Table 7 correspond to the location of the cooling tube (#1 to #6). This is due to the presence of a relatively thick layer of cooling fluid in those areas, and the fact that HFE-7000 has a relatively high-density (40% denser than water). Other areas with high RL contributions are at the locations of the taller standoffs for mounting of the high-mounted modules, particularly near the ID, since in that region, the support panel core is also replaced with solid plastic (or C-C) material because of the high density of pin holes and threaded holes in that area. Based on those estimates, local values of the RL contribution at normal incidence for a station range from about

1.8% in zone 8 (active area of one module, plus inactive area of another, plus the support panel), to almost 9.1% in zone 6 (where the cooling tube coincides with a tall thermal bridge on either side of the station and overlapping sensors and/or FPHX chips from both sides of the station).

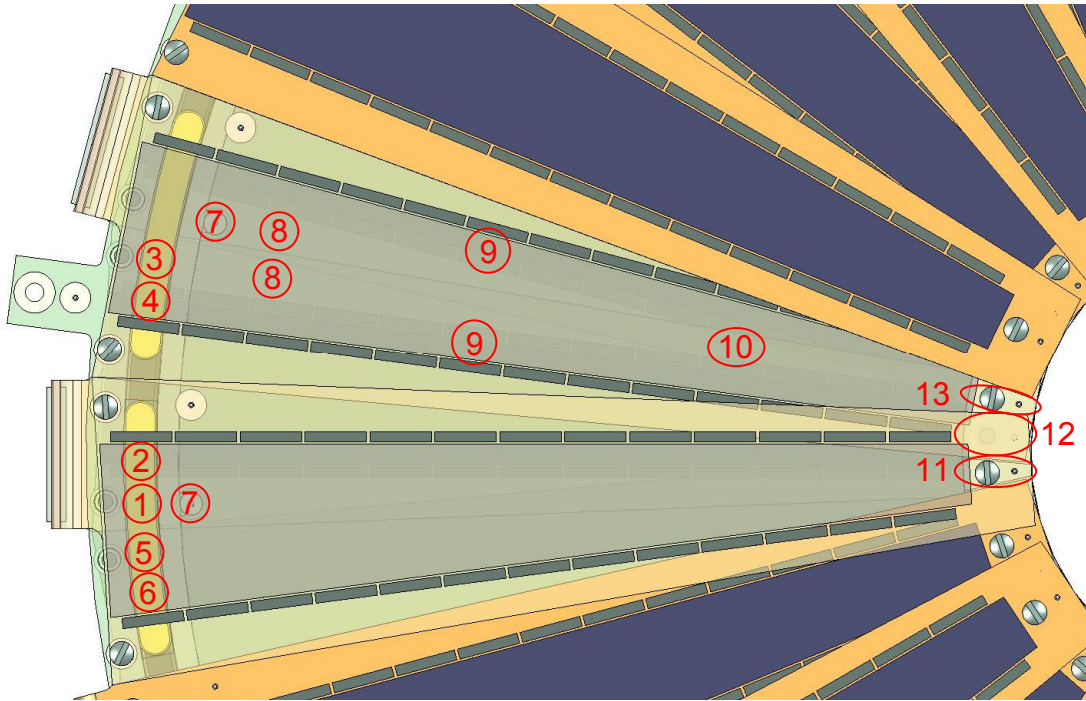


Figure 33: Representative regions for normal-incidence radiation length % for a single FVTX station (Station 2, 3, or 4 shown; all components made translucent for illustration purposes) .

| Region (Figure 33) | Stack | Normal incidence RL (%) |
|--------------------------|---|----------------------------|
| 1 | (S-B-HDI-B-BP)-SI-TB-B-(FS-B-T-CO-T-B-FS)-(BP-B-HDI) | 6.56% |
| 2 | (S-B-HDI-B-BP)-SI-TB-B-(FS-B-T-CO-T-B-FS)-SI-(BP-B-HDI-B-S) | 7.25% |
| 3 | (S-B-HDI-B-BP)-SI-(FS-B-T-CO-T-B-FS)-(BP-B-HDI) | 4.75% |
| 4 | (S-B-HDI-B-BP)-SI-(FS-B-T-CO-T-B-FS)-SI-(BP-B-HDI-B-S) | 5.44% |
| 5 | (S-B-HDI-B-BP)-SI-TB-B-(FS-B-C-B-FS)- (BP-B-HDI) | 6.56% |
| 6 | (S-B-HDI-B-BP)-SI-TB-B-(FS-B-C-B-FS)-B-TB-SI-(BP-B-HDI-B-S) | 9.06% |
| 7 | (S-B-HDI-B-BP)-(I-B-FS)-SO-(BP-B-HDI) | 4.43% |
| 8 | (S-B-HDI-B-BP)-(FS-B-C-B-FS)-(BP-B-HDI) | 1.80% |
| 9 | (S-B-HDI-B-BP)-(FS-B-C-B-FS)-(BP-B-HDI-B-S) | 2.15% |
| 10 | (S-B-HDI-B-BP)-(FS-B-C-B-FS)-(BP-B-HDI) ₂ | 2.34% |
| 11 | (HDI-B-BP)-SO-(FS-B-PC-B-FS)-SH-(BP-B-HDI) ₂ | 4.98% |
| 12 | (HDI-B-BP) ₂ -SH-(FS-B-PC-B-FS)-SH-(BP-B-HDI) | 3.85% |
| 13 | (HDI-B-BP)-SH-(FS-B-PC-B-FS)-SH-(BP-B-HDI) ₂ | 3.85% |

key: S=Sensor, B=Bond, HDI=High Density Interconnect, BP=BackPlane, T=Tube wall, C=Core, CO=COolant, I=Insert, TB=Thermal Bridge, SA=Silicone, RC=Readout Chip, SO=Stand-Off, SH=Shim (shallow version of SO), PC=Plastic Core
Parentheses are used to show logical groups (for ease of reading only)
subscripts are used to indicate multipliers for a layer or group

Table 7: Local extremes of normal incidence radiation length percentages for FVTX station 2, 3, or 4 (all-inclusive).

5.3 Radiation Hardness

The radiation environment specified for this detector system (Section 2.6.3) is very mild. Reference [33] contains a massive compilation of radiation damage to numerous materials. It was compiled by the European Center for Nuclear Research (CERN) and is an invaluable resource for design to these environments. A quick survey of that document reveals that almost none of the materials listed experiences a substantial reduction in useful properties as a result of exposure to a total dose of the order of 200kRads (2000Gy).

At 200kRads, the CERN document (its Appendices 5 and 6 : Summary Tables) suggests that, of the materials listed, the only one that should be considered problematic is Teflon. Other materials that may be marginal and deserve further research or testing are butyl rubber, cotton fiber, nylon, and chlorofluorocarbons (CFC's).

- Epoxies are shown to start experiencing property degradation at levels around 10^7 Gy, 4 orders of magnitude higher than the PHENIX environment.
- For Nylon, 60% reduction in fatigue life under repeated plastic deformation is cited after a total dose of 10^6 Gy. A yellow coloration was noted after a dose of 5×10^5 Gy (250 times the PHENIX dose), which is also the maximum recommended dose listed in Appendix 6 of ref. [33].
- Silicone rubber is shown to be essentially unaffected up to doses of the order of 50,000Gy, which is also the maximum recommend dose listed in Appendix 6, and is 25 times higher than the cumulative dose expected at PHENIX over a 10 year lifetime. Some data shows a 50% reduction in the elongation at break for doses above 2×10^5 Gy (100× the PHENIX dose) and complete embrittlement at a dose of 5×10^6 Gy (2500× the PHENIX dose).
- Specific data is not available for HFE-7000 (it was recently introduced on the market). The document (Appendix 5.5) indicates that CFC's and other fluorinated compounds may be an issue. Comparative testing of HFE-7000, before and after exposure to total doses around 200kRad (and higher), possibly also in contact with a qualified silicone rubber is highly recommended to discard the possibility of negative impact. Data may also be available on this subject from 3M (we have not yet investigated this).

5.4 Detector Module Performance

Based on the trade studies reported in Section 3, and as described in Section 3.2, the wedge backplane is made from a 0.762mm thick $[0/\pm 60]_{2s}$ quasi-isotropic K13C2U laminate. The temperature drop as predicted in the previous section is 4.3°C. Assuming a temperature of about 15°C at the back of the module (Section 4.5.2), the warmest read-out-chip will be operating at about 19.3°C which is consistent with the temperature requirements described in Section 2.10. Room temperature is assumed to be 21.1°C and thermal distortions are computed based on the temperature difference between room temperature and the expected steady-state temperature distribution of the wedge module.

Figure 34-a shows the assumed, best-fit quadratic temperature distribution on a 2-D wedge module with laminate elements. The wedge geometry in this figure is the final Z-staggered design presented in Section 4.3, which is wider than the initial design studied in the Section 3.2.

The increased width improves the flexural stiffness of the wedge as well as its thermal conduction. In this section, however, we only account for the improved stiffness and assume a conservative ΔT of 4.3°C .

Structural boundary conditions are three screw connections modeled by spiders of rigid elements. One screw is located approximately at a radius of 41mm and the remaining two are at a radius of 169mm^[19]. The deformed wedge module, with a maximum thermal distortion of $8.1\mu\text{m}$, is depicted in Figure 34-b where the wedge bows inwards (toward the support panel). Deformations due to the gravitational forces are neglected since wedge modules are installed in a vertical plane and gravity sag is negligible compared to thermal distortions.

The improvement in thermal distortions from $12.2\mu\text{m}$ in Table 4 to $8.1\mu\text{m}$ in the final design is attributed to the fact that the temperature load on the wedge was reduced by shifting the temperature profile by 2°C through edge cooling at 15°C rather than 13°C . Also, the increased surface area of the wedge has increased the stiffness of the wedge.

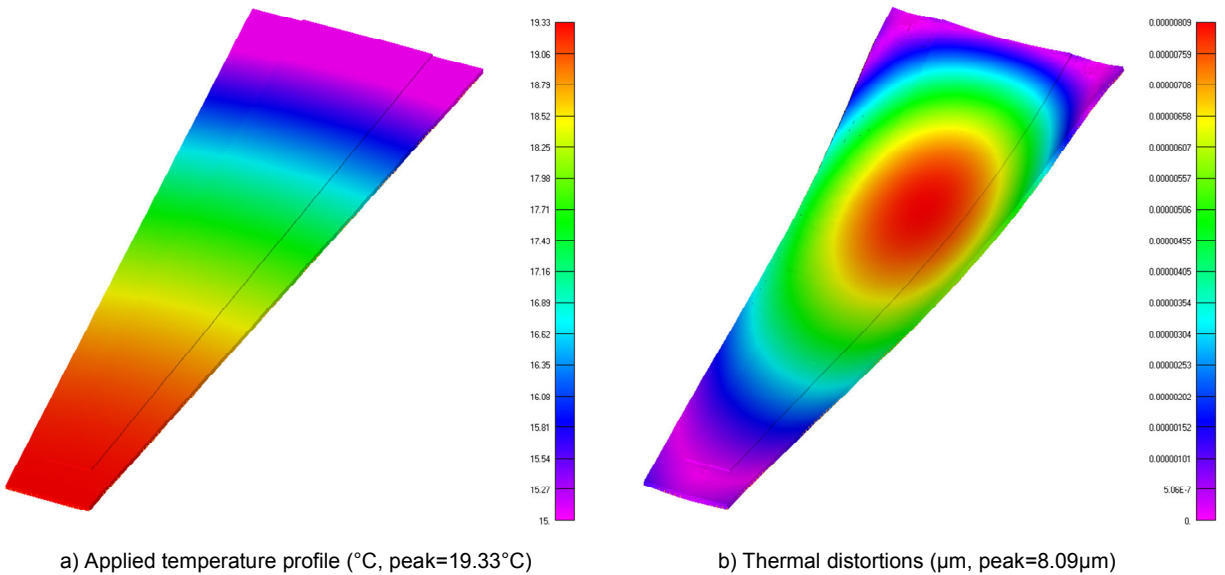


Figure 34: Thermal distortion of the wedge ($[0\pm60]_{2s}$ K13C2U Backplane, z-staggered design dimensions)

5.5 Half-Station Performance

In this section, thermal distortion of the final half disk assembly (stations 2 through 4) is studied. In the final design, wedge modules are staggered along the Z-axis^[21] and are wider than the initial design analyzed in Section 3.2.

The 2-D FE model prepared for the half disk assembly is shown in Figure 35-a. In this figure, the support panel (black) is the standard honeycomb sandwich plate, modeled using laminate elements. The detector regions of a wedge and the HDI regions are shown in gray and copper-red colors, respectively. On each side of the disk, there are 12 wedge modules connected to the support panel. In contrast to the half disk model studied in Section 3.3, the Z-staggered design has only one wedge which is not connected at all three screw connection points (see the wedge module at 12 o'clock position on the front in Figure 35-a).

The FVTX half-disk assembly is connected to the FVTX cage through three tabs approximately located at 12, 9, and 6 o'clock positions (see Figure 35-a). These connections are idealized as a simple support through a spider of nodes. The spider of rigid elements is approximately located at the physical screw locations and has a radius representative of the diameter of the screw head. Such idealization is depicted in Figure 35-b where rigid elements are shown in red. This idealization ignores the rotational stiffness of the cage and therefore will yield a conservative result.

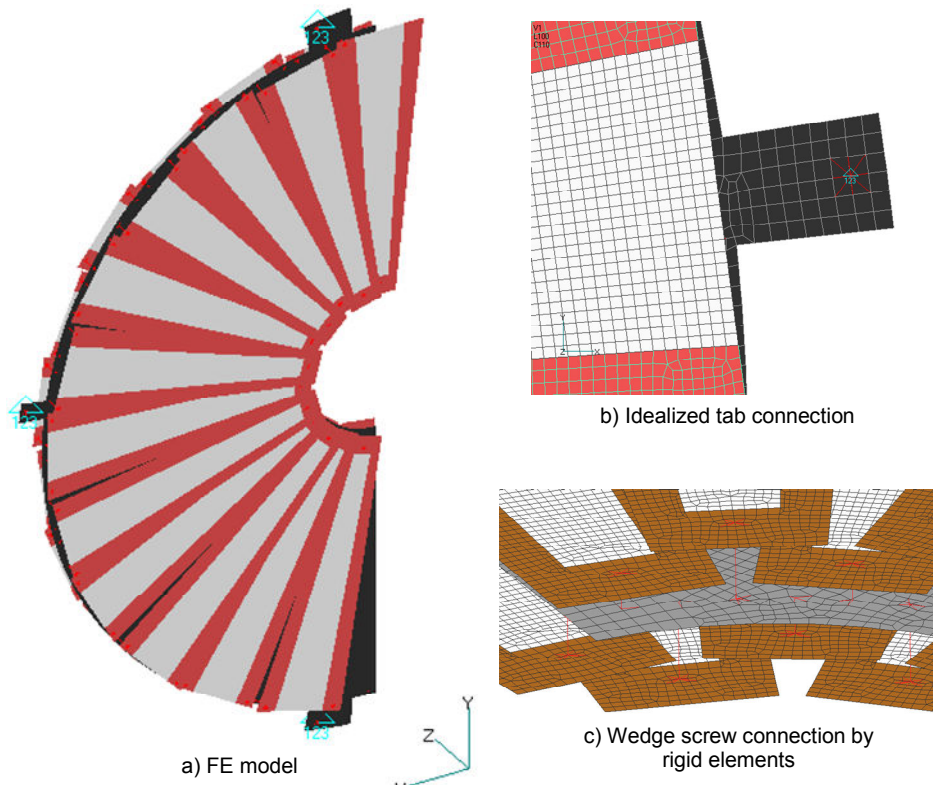


Figure 35: Half-disk assembly (Z-staggered wedge layout)

The applied temperature profile on the disk assembly is quadratic, similar to Section 3.3 with edge cooling at 15°C. The temperature contour is shown in Figure 36-a. Thermal distortion analysis with a reference temperature of 21.1°C predicts a maximum deformation along the Z axis of about 8 μm in the active detector region and a maximum total translation of 21 μm for the wedge at 12 o'clock position as shown in Figure 36-b. The dominant component of translation vector is along the z-axis (perpendicular to the disk). For simplicity total translation contour is depicted in Figure 36-b. A summary of the thermal distortions for stations 1 through 4 is given in Table 8.

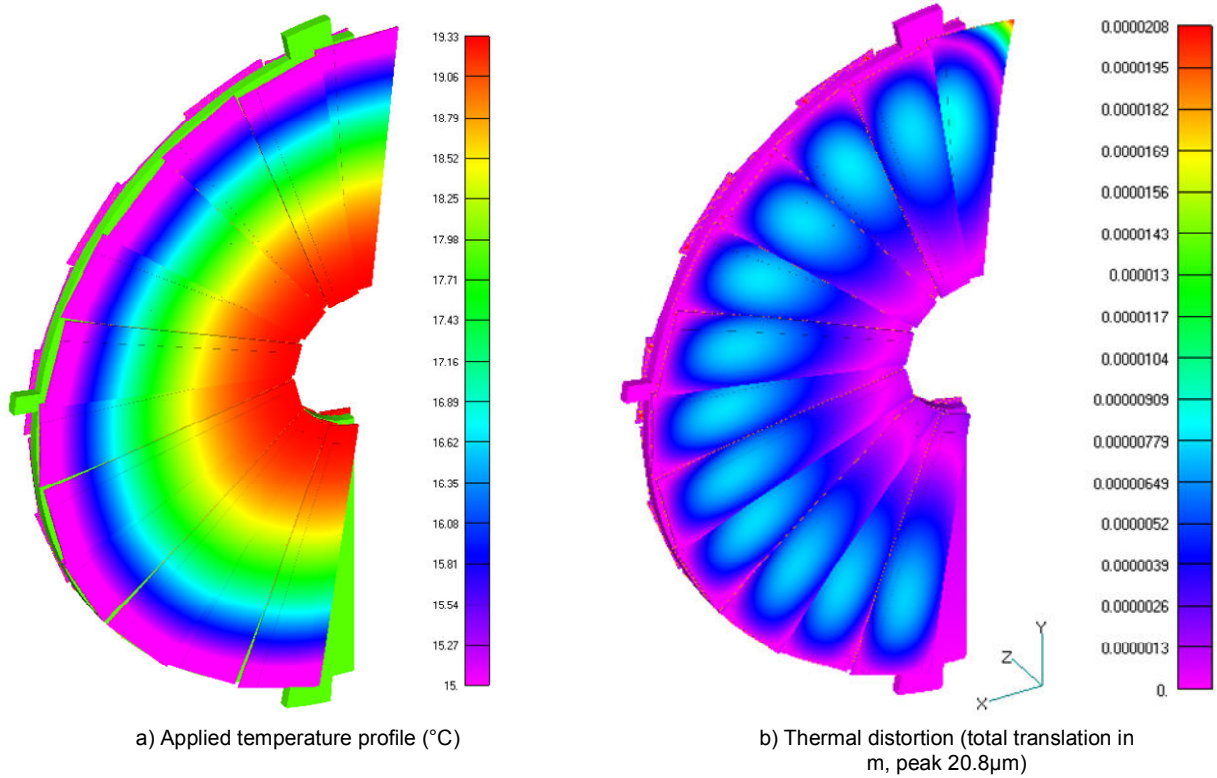


Figure 36: FVTX half-disk assembly with z-staggered wedge layout ([0/±60]_{2s} K13C2U wedge backplane, edge cooled to 15°C)

| Station | Absolute thermal distortions (microns) | | |
|----------|--|------|------|
| | X | Y | Z |
| 2 thru 4 | 0.43 | 0.27 | 8.00 |

Table 8: Thermal distortions of active area for FVTX half-disk assembly ([0/±60]_{2s} K13C2U wedge backplane, edge cooled to 15°C)

The natural frequency of the half-disk assembly with pin support is 120Hz. Higher modes occur at 250Hz, 320Hz, 347Hz, and 422Hz. We conclude that significant amplitudes of vibration in response to environmental excitations are unlikely to be a concern (also see Section 2.11).

5.6 FVTX Half-Station

Table 9 shows absolute deflection values for different stations due to the gravitational load in the $-Y$ direction. Variations in gravity sags as predicted in this table are primarily because of the cutout pattern in the cage structure. This can be improved by modifying the cutout pattern or even not having any cutout at all. This is a plausible option particularly since the cage material is not in the acceptance of the VTX/FVTX and therefore its radiation length is not a primary concern. For small deformations, the total translation of FVTX stations can be obtained by superimposing thermal distortions (Table 8) and gravity sag (Table 9). The deformed FVTX half-arm due to gravitational load in the $-Y$ direction, and the fundamental mode shape are depicted in Figure 37-a and Figure 37-b, respectively.

| Station | Absolute Gravity Sag (microns) | | |
|---------|--------------------------------|------|------|
| | X | Y | Z |
| 1 | 0.7 | 2.02 | 2.18 |
| 2 | 0.4 | 0.96 | 0.8 |
| 3 | 0.09 | 1.76 | 0.22 |
| 4 | 0.20 | 1.28 | 0.89 |

Table 9: Absolute gravity sag for FVTX stations (stand-alone analysis)

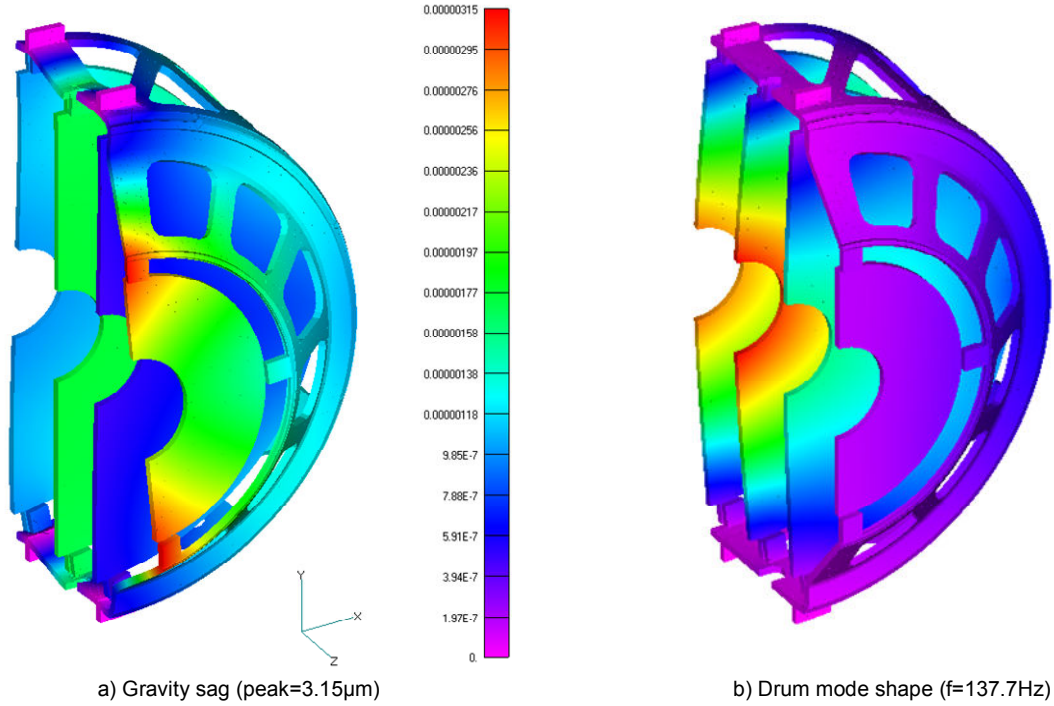


Figure 37: Gravity sag and fundamental vibration mode of the FVTX half-arm assembly.

5.7 VTX/FVTX System Level Analysis

In the previous section, a fundamental frequency of 138Hz was obtained for the FVTX module based on the assumption that cage tabs are pinned. In reality, FVTX modules are connected to the VTX space frame. In order to investigate the validity of a pinned connection, FVTX modules are connected to the space frame of the VTX system level FEM model (see Figure 38) previously developed by HYTEC^[37]. In this model, the VTX space frame is supported by kinematic mounts at top and bottom. The kinematic mounts are in turn assumed to be connected to rigid supports.

Free vibration analysis of the system level model predicts a fundamental frequency of 39Hz, dominated by lateral vibration of the barrel mounts (along X). The lowest mode that affects the FVTX is the 23rd mode, at a frequency of 99Hz.

In a parallel system level analysis by HYTEC^[40] kinematic mounts were connected to the existing isolation system (Aluminum support stand and rails) rather than rigid supports. It was

predicted there that the fundamental frequency of the entire system will drop to 24Hz in a mode driven by the support rails. Therefore, even though the VTX/FVTX assembly has a high enough frequency, with the current mounting system (whose design is out of HYTEC's scope) frequencies more than 24Hz cannot be achieved.

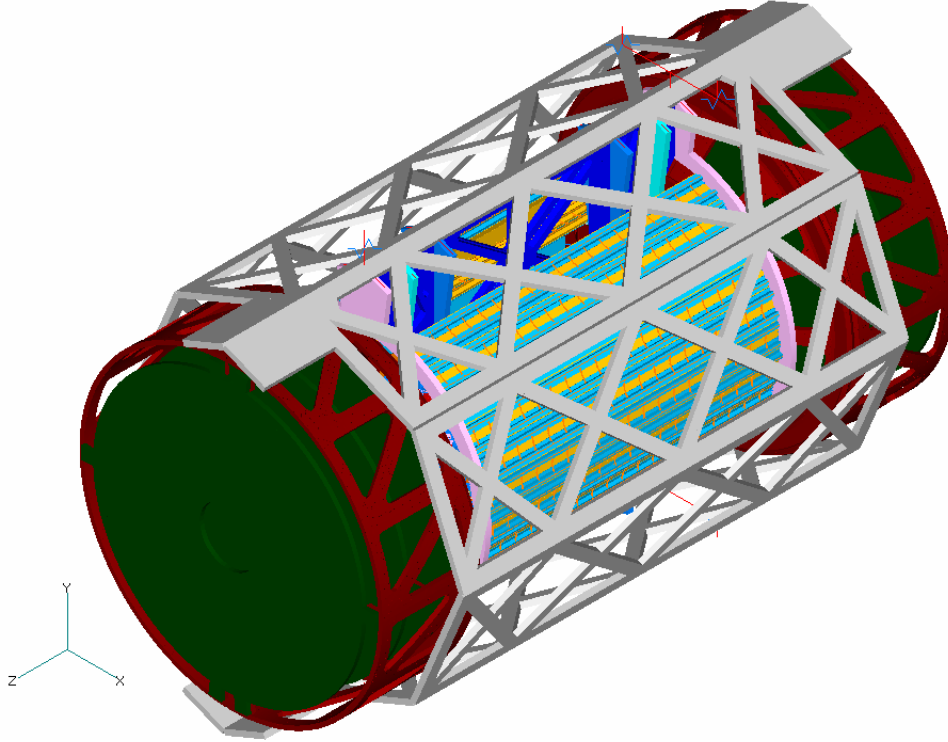


Figure 38: VTX/FVTX System level FEM model

In addition to vibrational analysis, gravity sag is also computed using the system level model. A summary of the absolute deflections due to gravity in $-Y$ direction (see Figure 38 for coordinate system definition) is given in Table 10. An estimate of the worst case total deflections due to combined gravity and thermal distortions can be computed by superimposing deflections from Table 8 and Table 10.

| Station | Absolute Gravity Sag (microns) | | |
|---------|--------------------------------|-------|------|
| | X | Y | Z |
| 1 | 0.41 | 11.96 | 0.69 |
| 2 | 3.84 | 18.48 | 3.15 |
| 3 | 0.81 | 11.82 | 3.23 |
| 4 | 1.93 | 15.53 | 3.08 |

Table 10: Absolute gravity sag for FVTX stations (system level analysis).

6. Conclusions

A fairly detailed preliminary design has been developed. Detailed material specifications (particularly in the area of adhesives) and final part dimensions remain to be defined, and are left for the final design phase.

The performance of the design has been evaluated via numerical simulations and closed-form analyses. The expected performance meets or exceeds radiation length (in an area-averaged sense), chip temperature, and dimensional stability requirements.

As a result of the decision to operate the gas enclosure at room temperature, temperature changes between assembly and operation of the detector modules are small. Consequently, stress levels in the silicon devices and the bonds are very comfortably low and allow the use of rigid adhesives throughout the assembly.

Natural frequencies have also been evaluated and are relatively high, easing concerns of flow-and/or environment-induced vibrations of amplitudes sufficient to disturb the precision alignment of the detectors. Flow-induced vibrations are difficult (at best) to estimate, so testing is recommended to validate this aspect of the design (see below). Specification of the acoustic and vibratory environments between the magnet poles was not available for analysis. It is recommended that such data be collected and analysis conducted to confirm the expected low amplitude of any dynamic deflections of the detector structures

The mechanical design is complicated by two key requirements:

- the presence of a pre-installed beam pipe and the resulting clam-shell design for the entire detector system, which cause difficulties with the support and cooling of individual sensor modules near the separation plane, and,
- the requirement that sensor modules be individually removable, which forces us to incorporate a large number of small fasteners and inserts in the station support panels; this is expected to have substantial impact of the cost of these structures.

As mentioned above, the area-averaged radiation length percentage of stations 2,3,4 (station 1 was not evaluated) meet the requirement, but locally large radiation length percentages are found in the general area of the cooling tubes, because of the relatively large volume of coolant. This is further aggravated by the need to stagger sensor modules on either side of the stations, and the tall standoffs required to implement this.

The cooling system design is very simple, owing to the low power levels, which allow us to rely on edge cooling alone. Also, arranging the four half-stations within each half-arm in series makes for a very simple and compact fluid distribution system (no manifolds).

The selection of a modern HFE coolant also mitigates concerns about leaks, since the coolant is completely harmless to electronics (even in liquid form), and benign to humans and the environment.

A few issues/concerns remain with the design that will need to be resolved in the final design phase; they are listed in Section 6.1.1.

Also, a number of aspects of the design have not yet been addressed, as they were outside the scope of this and related contracts. These are identified in Section 6.1.2

Finally, since the design currently relies entirely on analysis, prototyping and testing is recommended before committing to a fabrication program (details can be found in Section 6.2).

6.1 Remaining issues

6.1.1 Known issues and/or concerns with the preliminary design

- Flow-induced vibrations: turbulent fluid flow through the station support panels may produce sufficient excitation of elastic modes to make a significant contribution to the overall misalignment budget. This is very difficult to estimate by analysis. Testing is strongly recommended to evaluate this.
- The support and cooling of sensor modules at the edges of each half-station (near the separation plane) are less than optimal
 - Some edge modules are improperly cooled (one per half-station has no portion of the cooling tube at all underneath it). A possible solution may be to incorporate very high conductivity core and/or face sheet doublers in that area (tailored carbon-carbon perhaps). This would result in an additional, local increase in RL%.
- The HDI tails are too long for station 4. The tails are equipped with tandem, low profile connectors, which also require a G10 doubler to provide mechanical support during mating of the connectors. The connector section of the tail and mating extension cable cannot be bent. With their current length, coupled with the Z location of Station 4, the cables are pushed outside of our envelope.
- An interference^[11] between the FVTX cage and the ends of the ladders of VTX layer 4 has been identified (Figure 39). This has been communicated to the various groups collaborating on the project. Possible solutions include:
 1. move FVTX station 1 further away from IP in Z (by about 15mm)
 2. move VTX barrel 4 further out in radius (by about 10mm)
 3. shorten the length (i.e. along Z) of the VTX barrel 4 ladders (by about 10mm)
 4. redesign the FVTX support cage such that station 1 mounts to the outside (instead of the inside) of the cage)
 5. a combination of any or all of the above

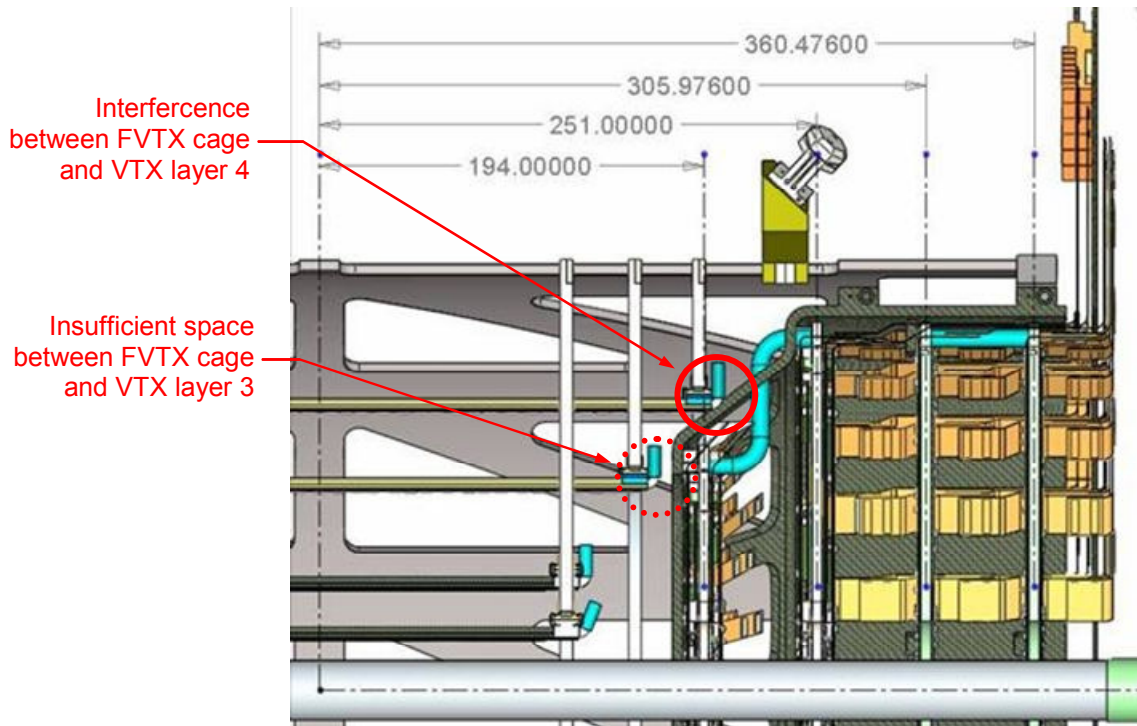


Figure 39: Interference between current FVTX design and VTX barrels.

6.1.2 Remaining tasks for final design phase

- Cage structure design: this design has not been detailed to the same level as the support panels and sensor modules. Final design details will need to be defined, and feasibility of the manufacturing approach (shaped sandwich panel) confirmed by contacting interested suppliers. Specific areas to be examined include:
 - feasibility of tight radii in a 3D sandwich shell,
 - how to make tabs, inserts, etc,
 - attachment details to VTX support frame,
 - possible redesign to solve interference with VTX (Section 6.1.1),
 - need for and exact design of cutouts.
- Support of readout cards (ROC) and routing/securing of cabling: to this day, the so-called “big-wheel” area has not received much design attention. This assembly represents a sizeable mass and dissipates significant power. A support structure must be designed, preferably in such a way that it is independent of the stable composite structures that support the sensors (possibly by attaching directly to the support stands, see Figure 2). Liquid cooling will also be required.
- Grounding of composite structures: the resin-based composites used throughout the design may not be sufficiently conductive to avoid the accumulation of electrical charge. Detector systems often require a fully conductive and grounded structures. Grounding requirements were not provided, and has not been incorporated in the design.
- Alignment features & surveying approach: precision pins have been designed into all joints to allow for precise alignment of components and subassemblies in the system.

Alignment will not be perfect however, and some combination of surveying and calibration will likely be required. This needs to be planned and requires coordination with other PHENIX detector systems and a good understanding of the available equipment and reference fiducials.

- Assembly tooling & procedures: at this point, only the assembly of the internal detector components is relatively well defined. Integration of the FVTX into the complete system and the fixtures and tooling required to achieve it have not received sufficient attention.
- Detailed material selections have, in many cases, not been finalized.

6.2 Recommended Future Work (Short Term)

6.2.1 Prototyping

The design is currently relying on analysis alone for performance predictions. Some of those predictions (thermal performance in particular) are based on rough approximations and would greatly benefit from experimental confirmation. Also, the intensity of vibrations that will be caused by turbulent flow of coolant within the stations cannot be easily predicted, and should be evaluated by testing. The following describes the type of prototypes and instrumentation that we would recommend.

6.2.1.1 Sensor module prototype:

A wedge prototype would consist of a composite backplane, with a prototype HDI bonded to it, a dummy silicon sensor (passive wafer of same thickness and in-plane dimensions as actual sensor, cut in the same crystalline orientation as the actual sensor), and resistive elements in place of the FPHX chips to simulate the local heat dissipation (simple surface mount resistances may be fine, given the low power).

This prototype would provide the following:

- Testing of assembly techniques and tooling (detailed design of the tooling, and prototypes would obviously be needed)
- Measurement of temperature drops in a dry Nitrogen environment. The wedge could be coupled to a copper cold-bar with liquid cooling. The entire test setup would be set inside of a temperature-controlled enclosure. Note that all equipment necessary for this test is already available at HYTEC.
- Optionally, temperature-induced distortions of the surface of the silicon dummy sensor could also be measured directly, using a computerized speckle pattern holography instrument available at HYTEC (PRISM).

6.2.1.2 Half-station prototype:

This would be a complete prototype of a half station support panel, populated with one to a few sensor module prototypes described in the previous section. The rest of the module locations could be populated with simpler, structural dummies (such as a simple backplane, made thicker to approximate the added stiffness and mass of the HDI and sensor).

This prototype could provide the following:

- Evaluation of manufacturability of the design and further refinement of insert designs and material selections.
- Validation of the feasibility of producing thin-walled nickel tubes with fittings.
- Better estimates of production costs from vendors.
- Validation of and practice with the module-to-station assembly concept, including the accuracy and repeatability of the alignment scheme (pins), the proper application of thermal interface beads, and module removal and replacement techniques.
- Direct measurement of flow induced vibrations (using simple accelerometers, and/or laser velocimeters, and/or speckle pattern holography PRISM), at various flow rates. Most of the equipment required for these tests is available at HYTEC.
- Heat transfer tests, performed in a controlled dry Nitrogen atmosphere.

6.2.1.3 Half-cage prototype

A prototype of this structure would be useful to evaluate feasibility of the manufacturing approach. However, we do not consider this as high a priority as the sensor module and half-station prototypes.

6.2.2 *Design:*

As mentioned previously, a number of design aspects have not yet been addressed. Some of the more pressing issues, in our view, are:

- Evaluate the manufacturing feasibility of the half-cage design. Key questions are related to tight radii and multiple-curvature in a molded sandwich structure. Short of a prototype, talks with interested vendors, and requesting ROM quotations would help us better understand the problem and refine the design.
- Solutions need to be developed and detailed to better support and cool the sensor modules at the edges of the half-stations.
- System level features:
 - Design of support structures and cooling system for the read-out cards, in the “big wheel” area.
 - Gas enclosure: a concept for this enclosure must be developed, in conjunction with VTX design activities. The concept will help us evaluate the total leakage area, and the flow rate of nitrogen required to maintain slight positive pressure in the enclosure.

6.2.3 *Other:*

- We need to identify one or more silicone tubing suppliers. The exact formulation of the silicone compound can greatly affect compatibility with our coolant. 3M may be able to help identify compatible tubing types. Accelerated exposure tests may also be required to confirm long-term durability of the tubing under exposure to the coolant.
- The impact of low-level radiation doses on our coolant has not been investigated. Once again, 3M may already have information available about this. If not, comparative testing of samples of the coolant before and after exposure to radiation (~200kRad dose) may be

indicated. Those tests may be best conducted in conjunction with tests on the silicone tubing.

7. Related HYTEC Documents

7.1 Presentation Slides

A number of status meetings and reviews were held during performance of this work. In most cases, slides were prepared to support those meeting. Those documents may help better understand the evolution of the design; they are listed in Table 11. These documents can be requested from the PHENIX project manager at HYTEC.

| Document Number | Title | Publication Date |
|-----------------|--|------------------|
| HPS-111006-0005 | PHENIX VTX – FVTX System Level FE Analysis Summary | 01/26/07 |
| HPS-111006-0006 | PHENIX FVTX Detector Plane Design Status | 02/06/07 |
| HPS-111006-0007 | PHENIX VTX – FVTX System Level FE Analysis Summary | 02/07/07 |
| HPS-111006-0008 | PHENIX FVTX Design Status | 02/23/07 |
| HPS-111006-0009 | PHENIX FVTX Wedge Trade Studies | 02/23/07 |
| HPS-111006-0010 | PHENIX FVTX Status of Mechanical and Thermal Design Work | 03/12/07 |

Table 11: List of FVTX-related documents produced by HYTEC.

7.2 Preliminary Drawing Package

This report is to be used in conjunction with the preliminary design package for the FVTX. This package contains top- and sub-assembly drawings with key dimensions, as well as preliminary part drawings for some of the better defined components. All these drawing are preliminary, identified as such on the face of the drawing, and should not be used for fabrication.

| Drawing Number | Revision level (at time of writing) | Title |
|-----------------|-------------------------------------|--|
| 111-PHX-01-1001 | | Phenix Central Upgrade – Sensor Locations |
| 111-PHX-01-3000 | | Phenix Central Upgrade – FVTX – Half-Arm Assembly |
| 111-PHX-01-3001 | C | Phenix Central Upgrade – FVTX Stations 2, 3, 4 – HDI Outline |
| 111-PHX-01-3002 | A | Phenix Central Upgrade – FVTX Stations 2 & 4 – Cooling Tube Weldment |
| 111-PHX-01-3003 | A | Phenix Central Upgrade – FVTX Station 3 – Cooling Tube Weldment |
| 111-PHX-01-3004 | A | Phenix Central Upgrade – FVTX Station 1 – Cooling Tube Weldment |
| 111-PHX-01-3005 | | Phenix Central Upgrade – FVTX – Cooling Hose Barb |
| 111-PHX-01-3006 | | Phenix Central Upgrade – FVTX Stations 2, 3, 4 – Sensor Module Assembly |
| 111-PHX-01-3007 | | Phenix Central Upgrade – FVTX Stations 2, 3, 4 – Detector Backplane |
| 111-PHX-01-3008 | | Phenix Central Upgrade – FVTX – Stations 1, 2, 3, & 4 – Support Panel Assembly |
| 111-PHX-01-3009 | | Phenix Central Upgrade – FVTX – Stations 2, 3, 4 – Assembly |
| 111-PHX-01-3010 | | Phenix Central Upgrade – FVTX – Half Cage |
| 111-PHX-01-3011 | A | Phenix Central Upgrade – FVTX – Readout Card Outline |
| 111-PHX-01-3012 | | Phenix Central Upgrade – FVTX Station 1 – Assembly |

Table 12: List of drawings included in the preliminary design package for the FVTX.

8. References

1. Melynda Brooks, "FVTX Design Document," Version 1, by e-mail, January 26, 2007.
2. Melynda Brooks, "FVTX Design Document," Version 2, by e-mail, April 5, 2007.
3. "Mechanical Specifications For PHENIX Central Magnet Region Detector Upgrades", on the PHENIX BNL website at http://www.phenix.bnl.gov/WWW/INTEGRATION/ME&Integration/mechanical_specifications.htm#Definitions%20and%20Coordinate%20systems, last updated February 21, 2007.
4. Walt Sondheim, "FVTX Detectors, 6in wafers", un-numbered LANL drawing, by e-mail, February 25, 2007.
5. David Lee, private communication, February 7, 2007.
6. Mark Prokop, E-mail and phone communications, February 5, 2007.
7. Mark Prokop, Melynda Brooks, and David Lee, orally, during technical meeting at HYTEC on March 15, 2007.
8. Melynda Brooks, orally, at FVTX collaboration meeting, UNM Physics department, Albuquerque, NM, March 12, 2007.
9. Walt Sondheim, FVTX Dictionary (VTX.FVTXDictionaryr1.4), by e-mail (copy of Twiki page), April 4, 2007.
10. W-M Yao *et al*, *Review of Particle Physics*, *J. Phys. G: Nucl. Part. Phys.* **33** 1, Table 6.1, pp. 104, 2006. Available electronically from the web site of the Particle Data Group at <http://pdg.lbl.gov/2006/html/downloads.html>
11. HYTEC drawing #111-PHX-01-1001, "Phenix Central Upgrade – Sensor Locations".
12. HYTEC drawing #111-PHX-01-3000, "Phenix Central Upgrade - FVTX – Half-Arm Assembly".
13. HYTEC drawing #111-PHX-01-3001, "Phenix Central Upgrade – FVTX Stations 2, 3, 4 – HDI Outline".
14. HYTEC drawing #111-PHX-01-3002-A, "Phenix Central Upgrade - FVTX Stations 2 & 4 – Cooling Tube Weldment".
15. HYTEC drawing #111-PHX-01-3003-A, "Phenix Central Upgrade - FVTX Station 3 – Cooling Tube Weldment".
16. HYTEC drawing #111-PHX-01-3004-A, "Phenix Central Upgrade - FVTX Station 1 – Cooling Tube Weldment".
17. HYTEC drawing #111-PHX-01-3005, "Phenix Central Upgrade - FVTX – Cooling Hose Barb".
18. HYTEC drawing #111-PHX-01-3006, "Phenix Central Upgrade - FVTX Stations 2, 3, 4 – Sensor Module Assembly".
19. HYTEC drawing #111-PHX-01-3007, "Phenix Central Upgrade - FVTX Stations 2, 3, 4 – Detector Backplane".
20. HYTEC drawing #111-PHX-01-3008, "Phenix Central Upgrade - FVTX Stations 1, 2, 3, & 4 - Support Panel Assembly".
21. HYTEC drawing #111-PHX-01-3009, "Phenix Central Upgrade - FVTX - Stations 2, 3, 4 Assembly".
22. HYTEC drawing #111-PHX-01-3010, "Phenix Central Upgrade - FVTX - Half Cage".

23. HYTEC drawing #111-PHX-01-3011, "Phenix Central Upgrade - FVTX – Readout Card Outline".
24. HYTEC drawing #111-PHX-01-3012, "Phenix Central Upgrade - FVTX – Station 1 Assembly".
25. HYTEC document #HPS-111006-0005, "PHENIX VTX – FVTX System Level FE Analysis Summary"
26. HYTEC document #HPS-111006-0006, "PHENIX FVTX Detector Plane Design Status"
27. HYTEC document #HPS-111006-0007, "PHENIX VTX-FVTX System Level FE Analysis Summary"
28. HYTEC document #HPS-111006-0008, "PHENIX FVTX Design Status"
29. HYTEC document #HPS-111006-0009, "PHENIX FVTX Wedge Trade Studies"
30. HYTEC document #HPS-111006-0010, "PHENIX FVTX Status of Mechanical and Thermal Design Work"
31. 3M Novec 7000 Engineered Fluid, Product Information Sheet #5045, 98-0212-2499-7, 3M Electronics, St Paul, MN (electronically available at http://products3.3m.com/catalog/us/en001/products/-/node_J8X6XQS1WRbe/root_GS2MT8MCQBgv/vroot_GS2MT8MCQBgv/gvel_22R1MWXS5Zgl/theme_us_oc_all_3_0/command_OCHandler/output_html).
32. "Fluorochemicals in Heat Transfer Applications, Frequently Asked Questions," 3M Electronics, St Paul, MN (electronically available from http://products3.3m.com/catalog/us/en001/products/-/node_J8X6XQS1WRbe/root_GS2MT8MCQBgv/vroot_GS2MT8MCQBgv/gvel_22R1MWXS5Zgl/theme_us_oc_all_3_0/command_OCHandler/output_html).
33. P. Beynel, P. Maier, and H. Schönbacher, "Compilation of Radiation Damage Test Data, Part III: Materials used Around High-Energy Accelerators, CERN doc. #82-10, November 1982.
34. R. F. Steidel Jr., D. D. Fuller, and J. W. Murdock, "Mechanics of Solids and Fluids," Section 3 of "Standard Handbook for Mechanical Engineers," 8th Ed., Baumeister et al., Eds, McGraw-Hill.
35. W. M. Kays and M. E. Crawford, "Convective Heat and Mass Transfer," 2nd Edition, McGraw-Hill (Series in Mechanical Engineering), 1980.
36. C. A. Sleicher and M. W. Rouse, International Journal of Heat and Mass Transfer, Vol. 17, pp. 677-683, 1975.
37. Stephens, V., FY06 PHENIX Structural Design/Analysis, and System Level FEM, HYTEC Inc. Report HTN-111006-0002, October 2006
38. Blevins, R.D., "Formulas for Natural Frequency and Mode Shape", Van Nostrand Reinhold , 1979
39. GE Advance Ceramics, TPG Thermal Management Material, Pub. No 85505 Rev. 2, September 2003
40. HPS-111006-0005 "PHENIX VTX-FVTX, System Level FE Analysis Summary", HYTEC Inc., January 26. 2007

9. Acronyms

| | |
|------|---|
| ASIC | Application Specific Integrated Circuit |
| BNL | Brookhaven National Laboratory |

| | |
|--------|--|
| CAD | Computer Aided Design |
| C-C | Carbon-Carbon |
| CE | Cyanate Ester |
| CERN | Centre Européen pour la Recherche Nucléaire |
| CFC | Chloro-Fluoro-Carbon |
| CLT | Classical Lamination Theory |
| CTE | Coefficient of Thermal Expansion (linear) |
| DI | DeIonized (water) |
| DOF | Degree Of Freedom |
| FEM | Finite Element Model |
| FE(M) | Finite Element (Model) |
| FPHX | designates the readout chip used on the FVTX sensor module |
| FVTX | Forward VerTeX Detector |
| GR | Graphite |
| HDI | High Density Interconnect |
| HFE | HydroFluoroEther |
| IP | Interaction Point |
| OD | Outer Diameter |
| PHENIX | Pioneering High Energy Interaction eXperiment |
| Q-I | Quasi-Isotropic |
| RHIC | Relativistic Heavy-Ion Collider |
| RL | Radiation Length |
| TPG | Thermal Pyrolytic Graphite |
| VTX | VerTeX Detector |

Appendix A. Material properties used in models

Materials studied for the wedge backplane are encapsulated TPG and Graphite/Cyanate uni-directional composites M55J/954-3 and K13C2U/RS-3C. Typical properties used in the numerical simulation for these components are given in Table 14^[39,37]. Material properties for other layers in the wedge stack-up are also given in Table 14. The support panel is a sandwich plate with high performance Aluminum honeycomb core (HEXCEL 3/16-5056-0.0007, 2.0 lb/ft³) and QI symmetric [0/45/90/-45]_s M55J/954-3 facesheets for which material properties are listed.

Effective in-plane properties for different backplane layups as well as for the sandwich support panel are given in Table 15. These effective properties provide a comparative measure of different lay-ups in stiffness, coefficient of thermal expansion, and thermal conductivity.

| Backplane lay-up | Thickness | K _x | K _y | K _z |
|--|-----------|----------------|----------------|----------------|
| | mm | | | |
| [0/45/90/-45] _s | 0.508 | 179.4 | 179.4 | 0.8 |
| [0/45/90/-45] _{2s} | 1.016 | 179.4 | 179.4 | 0.8 |
| | | | | |
| [0/±60] _s | 0.381 | 179.4 | 179.4 | 0.8 |
| [0/±60] _{2s} | 0.762 | 179.4 | 179.4 | 0.8 |
| | | | | |
| [0 ₂ /45/90/-45] _s | 0.635 | 215.1 | 143.7 | 0.8 |
| [0 ₂ /45/90 ₂ /-45] _s | 0.762 | 179.4 | 179.4 | 0.8 |
| | | | | |
| [40/0/-40/0] _s | 0.508 | 284.2 | 74.6 | 0.8 |
| [40/0/-40/0] _{2s} | 1.016 | 284.2 | 74.6 | 0.8 |

Table 13: Effective thermal conductivities for K13C2U backplanes with different layups and thicknesses.

| | t | ρ | E_1 | E_2 | E_3 | ν_{12} | G_{12} | G_{23} | G_{13} | α_1 | α_2 | α_3 | K_1 | K_2 | K_3 |
|----------------------|--------|-------------------|-------|-------|-------|------------|----------|----------|----------|------------|------------|------------|--------|--------|-------|
| | mm | Kg/m ³ | GPa | GPa | GPa | | GPa | GPa | GPa | ppm/°K | ppm/°K | ppm/°K | W/mK | W/mK | W/mK |
| TPG | 0.2460 | 2260.0 | 827.4 | 827.4 | 34.5 | 0.30 | 318.1 | 1.0 | 1.0 | -1.00 | -1.00 | 25.00 | 1500.0 | 1500.0 | 10.0 |
| M55J/954-3 | 0.0635 | 1633.1 | 312.3 | 6.9 | 6.9 | 0.30 | 4.5 | 2.8 | 4.5 | -0.63 | 22.40 | 22.4 | 69.2 | 0.8 | 0.8 |
| K13C2U/RS-3C | 0.0635 | 1799.2 | 528.1 | 6.9 | 6.9 | 0.38 | 4.9 | 1.1 | 4.9 | -0.94 | 28.14 | 28.14 | 358.0 | 0.8 | 0.8 |
| Kapton-Cu Laminate | 0.1760 | 2225.0 | 17.5 | 17.5 | 3.4 | 0.30 | 6.6 | 1.3 | 1.3 | 17.30 | 17.30 | 24.90 | 49.3 | 49.3 | 0.2 |
| FPHX Chip | 0.3000 | 2330.0 | 110.0 | 110.0 | 110.0 | 0.28 | 43.0 | 43.0 | 43.0 | 2.60 | 2.60 | 2.60 | 150.0 | 150.0 | 150.0 |
| Silicon Detectors | 0.3000 | 2330.0 | 110.0 | 110.0 | 110.0 | 0.28 | 43.0 | 43.0 | 43.0 | 2.60 | 2.60 | 2.60 | 150.0 | 150.0 | 150.0 |
| Aluminum HC Core | 4.7625 | 32.0 | 0.0 | 0.0 | 0.3 | 0.4 | 0.0 | 0.1 | 0.2 | 18.48 | 18.48 | 18.48 | 0.7 | 0.3 | 1.4 |
| Non-conductive Epoxy | 0.1000 | 1200.0 | 2.5 | 2.5 | 2.5 | 0.30 | 1.0 | 1.0 | 1.0 | 50.00 | 50.00 | 50.00 | 0.2 | 0.2 | 0.2 |
| Conductive Epoxy | 0.1000 | 2300.0 | 14.0 | 14.0 | 14.0 | 0.3 | 5.4 | 5.4 | 5.4 | 25.00 | 25.00 | 25.00 | 1.5 | 1.5 | 1.5 |
| Conductive Silicone | 1.000 | 2450.0 | 0.005 | 0.005 | 0.005 | 0.49 | 0.002 | 0.002 | 0.002 | 104.0 | 104.0 | 104.0 | 1.7 | 1.7 | 1.7 |

Table 14: Typical lamina properties.

| | t | ρ | E_1 | E_2 | ν_{12} | G_{12} | α_1 | α_2 | α_3 | K_1 | K_2 | K_3 |
|---|-------|-------------------|-------|-------|------------|----------|------------|------------|------------|-------|-------|-------|
| | mm | Kg/m ³ | GPa | GPa | | GPa | ppm/°C | ppm/°C | ppm/°K | W/mK | W/mK | W/mK |
| Encapsulated TPG backplane | 0.500 | 1941.5 | 494.0 | 494.0 | 0.2559 | 158.8 | -0.875 | -0.875 | 25.0 | 755.8 | 755.8 | 1.5 |
| [0/45/90/-45] _s K13C2U backplane | 0.508 | 1799.2 | 182.2 | 182.2 | 0.3258 | 68.7 | -0.425 | -0.425 | 24.0 | 179.4 | 179.4 | 0.8 |
| [0/45/90/-45] _s M55J backplane | 0.508 | 1633.1 | 110.1 | 110.1 | 0.3202 | 41.7 | 0.008 | 0.008 | 22.4 | 35.0 | 35.0 | 0.8 |
| Sandwich Support Panel | 5.270 | 186.4 | 106.2 | 106.2 | 0.3200 | 4.0 | 0.008 | 0.008 | - | 4.0 | 3.6 | 1.3 |

Table 15: Effective inplane properties based on CLT.

Appendix B. Mass properties

Mass properties for different components of the FVTX module are listed in Table 16. Wedge backplane is K13C2U composite with quasi-isotropic $[0/\pm 60]_{2s}$ layup. In this table, mass of the cooling fluid (3M Novec HFE-7000) is approximately included for the half disk assembly as well. Approximate mass of the entire VTX/FVTX assembly computed from the system level model (see Section 5.7) is 18.11Kg.

| | Mass (gr) | Comments |
|---|-----------|--|
| Wedge Module (stations 2 thru 4) | 8.95 | |
| Half Disk Assembly (stations 2 thru 4) | 274.1 | support panel, 24 wedge modules, and cooling fluid |
| Cage | 72.0 | |
| Half Cage Assembly | 1021.5 | |

Table 16 FVTX mass properties

Appendix C. 2-D vs. 3-D Wedge Results

Wedge models presented in Section 3.2 are primarily intended for steady-state heat transfer analysis. A 3-D model with effective in-plane properties for the backplane cannot accurately predict thermal distortions since for composite laminates effective *bending* stiffness could be different from effective *in-plane* stiffness. A more realistic 3-D representation of the wedge would be defining at least a layer of solid elements for each physical layer in the laminate stack-up with its corresponding orientation angle. This would be prohibitive because of computational costs and therefore impractical for different trade studies. In this section, however, a layer by layer 3-D model is presented only to validate 2-D analysis results using laminate elements. Figure 40 shows a close up of the 3-D layer by layer mesh for a $[0/45/90/-45]_s$ backplane.

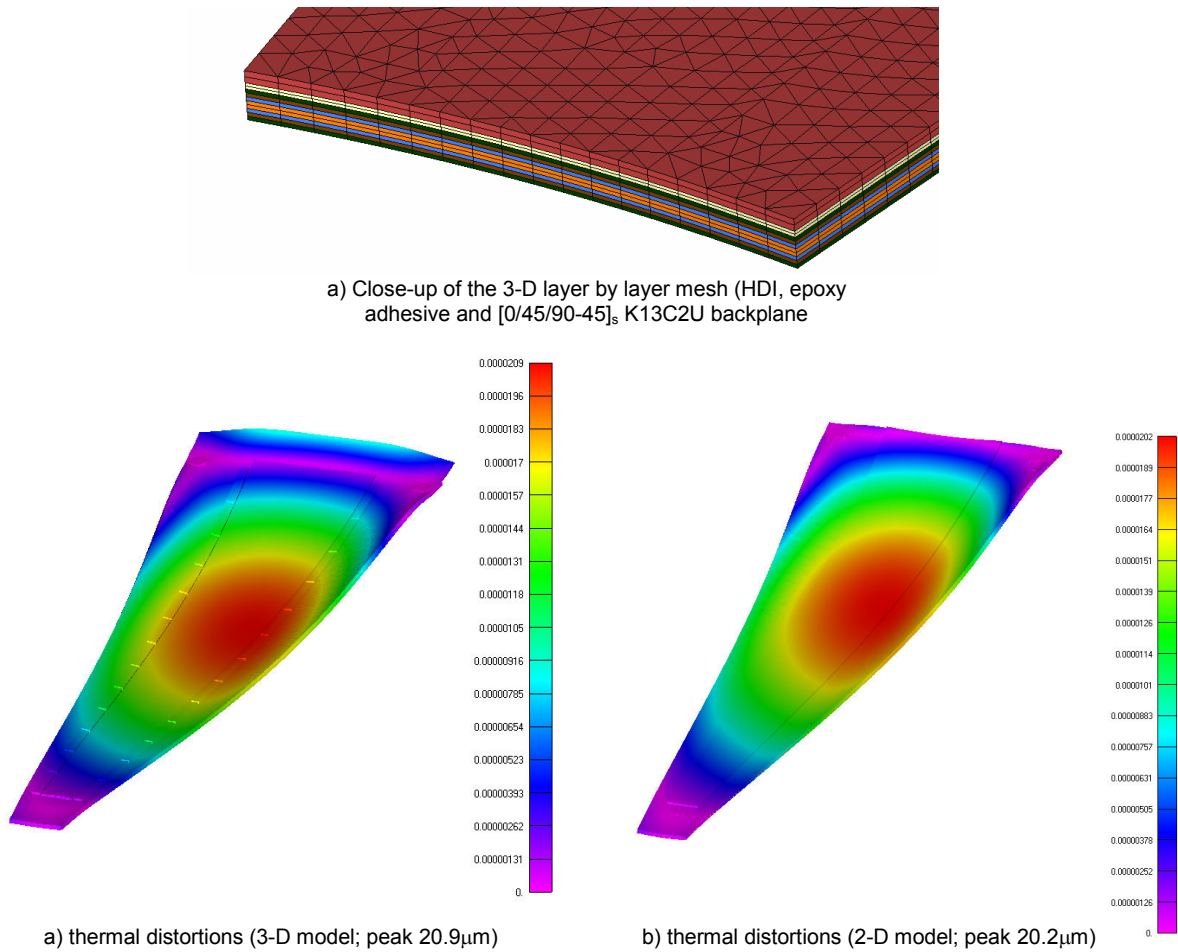


Figure 40: 3-D vs. 2-D Wedge models ($[0/45/90-45]_s$ K13C2U backplane; 13C edge cooled)

An important modeling aspect is correct representation of the screw connections in the FEM models. Numerical studies reveal that for the order of thermal distortions relevant to the wedge design boundary conditions can have a significant impact on the magnitude of the thermal distortions. Since plastic screws are used to fasten wedge modules to the support panel, the actual physical boundary condition is best simulated by fixing a group of nodes on the backside

of the thermal backplane for each screw connection as shown in Figure 9. This, however, cannot be replicated using plate elements since only one node is defined through the thickness of plate elements.

For validation purposes, we modify boundary conditions applied on the 3-D model to be similar to that of the 2-D model. This is done by fixing a group of nodes representative of the screw head through the thickness of the model. Thermal distortions for this type of boundary condition is depicted in Figure 40-b which compares very well with its 2-D counter part shown in Figure 40-c. We conclude that 2-D laminate elements are valid for the thermal distortion studies presented in this report, however, they tend to under predict thermal distortions since boundary condition cannot be correctly simulated. To account for this discrepancy it is recommended that appropriate margins of safety be considered in designs when using 2-D analysis results.

Appendix D. Analytical Validations

In order to validate the numerical result obtained by FEM simulations, simplified cases are studied for which analytical results can be obtained. In the following sections, steady-state heat transfer and free vibration analysis of an equivalent wedge are compared with FEM results.

Steady State Heat Transfer

Consider the steady-state heat transfer problem for the wedge with uniform heat generation and edge cooling. This can be simplified to a 1-D heat transfer problem with equivalent properties. The temperature distribution then can be obtained by solving the following ODE with appropriate boundary conditions for $0 \leq x \leq L$

$$\frac{d^2 T}{dx^2} + \frac{q}{k} = 0 \quad (8)$$

in which T is temperature as function of position x , q is the input heat, and k is the thermal conductivity. We consider a 1-D bar with representative dimensions $0.1239\text{m} \times 0.0268\text{m} \times 0.0012\text{m}$. For boundary conditions $T(x) = T_0$ at $x = 0$ and $dT(x)/dx = 0$ at $x = L$; the solution of Equation (1) takes a quadratic form from which temperature at $x = L$ is computed to be

$$T(L) = T_0 + \frac{qL^2}{2k} \quad (9)$$

The calculated effective inplane thermal conductivity of the stack-up given in Table 17 is $k=101.15\text{W/mK}$. Input heat is assumed to be uniform through out the length of the effective 1-D model generated by 26 FPHX chips each wasting 0.0128W of heat. This translate into a uniform heat generation of $q=83.5\text{kW/m}^3$. Substituting the effective values in Equation (2) the maximum temperature of 19.33°C is predicted which is in very good agreement with the FEM results of 19.91°C as reported in Table 7.

| | In-plane Thermal Conductivity | Thickness |
|----------------------|----------------------------------|-----------|
| | W/mK | mm |
| K13C2U Laminate | 130 | 0.508 |
| Non-Conductive Epoxy | 0.2 | 0.100 |
| Kapton Bus | 49.33 | 0.176 |
| Non-Conductive Epoxy | 0.2 | 0.100 |
| Silicon Detector | 150 | 0.300 |

Table 17: Effective thermal wedge stack-up

Free Vibration

The wedge natural frequency obtained using the FEM model is compared with natural frequency of a rectangular plate. This plate is 0.1239m long, 0.0268m wide, and 0.508mm thick and assumed to be made of the K13C2U backplane only. The natural frequency in this case can be calculated using the following simple relation^[38]

$$f = \frac{\lambda_{ij}}{2\pi a^2} \left[\frac{Eh^3}{12\gamma(1-\nu^2)} \right] \quad (10)$$

where λ_{ij} is a dimensionless frequency parameter which is a function of boundary conditions and aspect ratio^[38], E is the modulus of elasticity, ν is the Poisson's ratio, h is the plate thickness, γ is mass per unit area, and a is the plate length. Table 18 lists natural frequency for the effective wedge for two separate boundary conditions; two opposite edges clamped (CCFF) and two opposite edges simply supported while the other two are free. These frequencies are consistent with the frequency of 366Hz obtained by FEM analysis (see Table 7). Moreover, this table implies that the wedge screw connections are closer to clamped edge conditions than a simply supported one.

| Boundary Condition | λ_{ij} | f (Hz) |
|--------------------|----------------|--------|
| CCFF | 21.9 | 354.27 |
| SSFF | 9.0 | 145.59 |

Table 18: Analytical natural frequency of the equivalent wedge.

Appendix E. Statement of Work

Statement of Work, Contract with HYTEC INC

The subcontractor shall produce a design package for the forward-silicon-vertex-detector (FVTX) that will be a part of the PHENIX collider detector at Brookhaven National Laboratory. This detector must be integrated with the existing central silicon vertex barrel detector system (VTX). The following are a list of tasks that are covered under this contract. The completion of these tasks by HYTEC, during FY06 and FY07, will lead to the successful installation of the FVTX endcap detectors into the VTX system.

1, The full FVTX mounting system design; this will be in two phases, a R&D phase and a design phase. The R&D part will include mechanical and thermal analysis of the GFRP (Graphite) support frame. This is a similar structure as was used in the ATLAS vertex detector, which was also designed by HYTEC. Determine finite analysis (FEA) to determine dynamic stiffness. Perform FEA for mass-loaded static stiffness, to insure less than 100. microns of sag due to gravity. Optimize the mass for radiation length, structural integrity and access. Optimize the location and shape of mass reducing cutouts.

Design a sandwich GFRP composite structure to meet dimensional and structural stability (DSS) and gravitational structural stability (GSS) specifications. Use stiffening structural end plates as required.

2, Cooling; The eight planes of silicon disks will need to be cooled in order to remove the heat load generated from the attached read-out electronics chips. This cooling system will be operated at 0 degrees Centigrade, similar to the VTX cooling system. The existing system will be designed to incorporate the additional heat load generated by the FVTX system. A per-fluorocarbon fluid will be used as the coolant. All materials must be compatible with this coolant.

3, Project Management; HYTEC will provide weekly e-mail updates and monthly reviews throughout the contract. The FVTX team will meet weekly to discuss issues and review progress.

4, M&S and travel; member of the HYTEC team will travel to BNL and LANL as required.